Chapter 10 Phase Transformations: Development of Microstructure and Alteration of Mechanical Properties

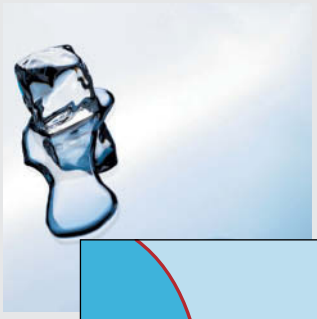

SuperStock

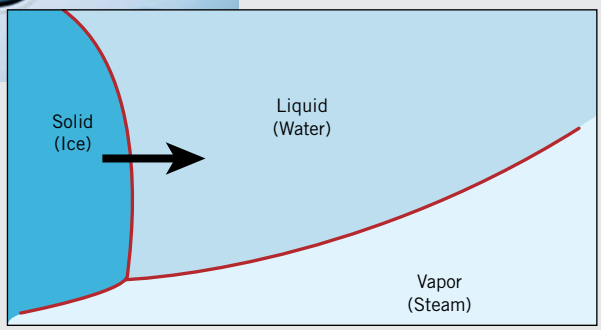

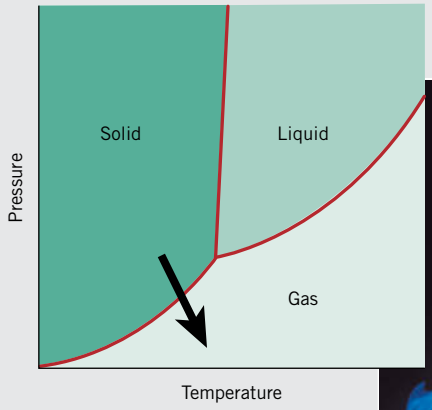

Charles D. Winters/Photo Researchers, Inc.

Two pressure–temperature phase diagrams are shown: for H_2O (top) and CO_2 (bottom). Phase transformations occur when phase boundaries (the red curves) on these plots are crossed as temperature and/or pressure is changed. For example, ice melts (transforms to liquid water) upon heating, which corresponds to crossing the solid-liquid phase boundary, as represented by the arrow on the H_2O phase diagram. Similarly, upon passing across the solid-gas phase boundary of the CO_2 phase diagram, dry ice (solid CO_2) sublimes (transforms into gaseous CO_2). Again, an arrow delineates this phase transformation.

WHY STUDY *Phase Transformations*?

The development of a set of desirable mechanical characteristics for a material often results from a phase transformation that is wrought by a heat treatment. The time and temperature dependencies of some phase transformations are conveniently represented on modified phase diagrams. It is important to know how to use these diagrams in order to design a heat treatment for some alloy that will yield the desired room-temperature mechanical properties. For example, the tensile strength of an iron–carbon alloy of eutectoid composition (0.76 wt% C) can be varied between approximately 700 MPa (100,000 psi) and 2000 MPa (300,000 psi) depending on the heat treatment employed.

Learning Objectives

After studying this chapter, you should be able to do the following:

1. Make a schematic fraction transformation-versus-logarithm of time plot for a typical solid–solid transformation; cite the equation that describes this behavior.
2. Briefly describe the microstructure for each of the following microconstituents that are found in steel alloys: fine pearlite, coarse pearlite, spheroidite, bainite, martensite, and tempered martensite.
3. Cite the general mechanical characteristics for each of the following microconstituents: fine pearlite, coarse pearlite, spheroidite, bainite, martensite, and tempered martensite; briefly explain these behaviors in terms of microstructure (or crystal structure).
4. Given the isothermal transformation (or continuous-cooling transformation) diagram for some iron–carbon alloy, design a heat treatment that will produce a specified microstructure.

10.1 INTRODUCTION

One reason metallic materials are so versatile is that their mechanical properties (strength, hardness, ductility, etc.) are subject to control and management over relatively large ranges. Three strengthening mechanisms were discussed in Chapter 7—namely grain size refinement, solid-solution strengthening, and strain hardening. Additional techniques are available in which the mechanical behavior of a metal alloy is influenced by its microstructure.

The development of microstructure in both single- and two-phase alloys typically involves some type of phase transformation—an alteration in the number and/or character of the phases. The first portion of this chapter is devoted to a brief discussion of some of the basic principles relating to transformations involving solid phases. Because most phase transformations do not occur instantaneously, consideration is given to the dependence of reaction progress on time, or the **transformation rate.** This is followed by a discussion of the development of two-phase microstructures for iron–carbon alloys. Modified phase diagrams are introduced that permit determination of the microstructure that results from a specific heat treatment. Finally, other microconstituents in addition to pearlite are presented and, for each, the mechanical properties are discussed.

transformation rate

Phase Transformations

10.2 BASIC CONCEPTS

phase transformation

A variety of **phase transformations** are important in the processing of materials, and usually they involve some alteration of the microstructure. For purposes of this discussion, these transformations are divided into three classifications. In one group are

simple diffusion-dependent transformations in which there is no change in either the number or composition of the phases present. These include solidification of a pure metal, allotropic transformations, and recrystallization and grain growth (see Sections 7.12 and 7.13).

In another type of diffusion-dependent transformation, there is some alteration in phase compositions and often in the number of phases present; the final microstructure typically consists of two phases. The eutectoid reaction described by Equation 9.19 is of this type; it receives further attention in Section 10.5.

The third kind of transformation is diffusionless, in which a metastable phase is produced. As discussed in Section 10.5, a martensitic transformation, which may be induced in some steel alloys, falls into this category.

10.3 THE KINETICS OF PHASE TRANSFORMATIONS

With phase transformations, normally at least one new phase is formed that has different physical/chemical characteristics and/or a different structure than the parent phase. Furthermore, most phase transformations do not occur instantaneously. Rather, they begin by the formation of numerous small particles of the new phase(s), which increase in size until the transformation has reached completion. The progress of a phase transformation may be broken down into two distinct stages: **nucleation** and **growth.** Nucleation involves the appearance of very small particles, or nuclei of the new phase (often consisting of only a few hundred atoms), which are capable of growing. During the growth stage, these nuclei increase in size, which results in the disappearance of some (or all) of the parent phase. The transformation reaches completion if the growth of these new-phase particles is allowed to proceed until the equilibrium fraction is attained. We now discuss the mechanics of these two processes and how they relate to solid-state transformations.

nucleation, growth

Nucleation

There are two types of nucleation: *homogeneous* and *heterogeneous*. The distinction between them is made according to the site at which nucleating events occur. For the homogeneous type, nuclei of the new phase form uniformly throughout the parent phase, whereas for the heterogeneous type, nuclei form preferentially at structural inhomogeneities, such as container surfaces, insoluble impurities, grain boundaries, dislocations, and so on. We begin by discussing homogeneous nucleation because its description and theory are simpler to treat. These principles are then extended to a discussion of the heterogeneous type.

Homogeneous Nucleation

A discussion of the theory of nucleation involves a thermodynamic parameter called **free energy** (or *Gibbs free energy*), G. In brief, free energy is a function of other thermodynamic parameters, of which one is the internal energy of the system (i.e., the *enthalpy, H*) and another is a measurement of the randomness or disorder of the atoms or molecules (i.e., the *entropy, S*). It is not our purpose here to provide a detailed discussion of the principles of thermodynamics as they apply to materials systems. However, relative to phase transformations, an important thermodynamic parameter is the change in free energy ΔG; a transformation occurs spontaneously only when ΔG has a negative value.

free energy

For the sake of simplicity, let us first consider the solidification of a pure material, assuming that nuclei of the solid phase form in the interior of the liquid as atoms cluster together so as to form a packing arrangement similar to that found in the solid phase.

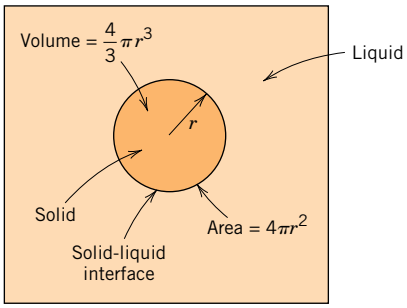

Figure 10.1 Schematic diagram showing the nucleation of a spherical solid particle in a liquid.

Furthermore, it will be assumed that each nucleus is spherical and has a radius r. This situation is represented schematically in Figure 10.1.

There are two contributions to the total free energy change that accompany a solidification transformation. The first is the free energy difference between the solid and liquid phases, or the volume free energy, ΔG_v. Its value is negative if the temperature is below the equilibrium solidification temperature, and the magnitude of its contribution is the product of ΔG_v and the volume of the spherical nucleus (i.e., $\frac{4}{3}\pi r^3$). The second energy contribution results from the formation of the solid–liquid phase boundary during the solidification transformation. Associated with this boundary is a surface free energy, γ, which is positive; furthermore, the magnitude of this contribution is the product of γ and the surface area of the nucleus (i.e., $4\pi r^2$). Finally, the total free energy change is equal to the sum of these two contributions:

Total free energy change for a solidification transformation

$$\Delta G = \tfrac{4}{3}\pi r^3 \Delta G_v + 4\pi r^2 \gamma \tag{10.1}$$

These volume, surface, and total free energy contributions are plotted schematically as a function of nucleus radius in Figures 10.2*a* and 10.2*b*. Figure 10.2*a* shows that for the curve corresponding to the first term on the right-hand side of Equation 10.1, the free energy (which is negative) decreases with the third power of r. Furthermore, for the curve resulting from the second term in Equation 10.1, energy values are positive and increase with the square of the radius. Consequently, the curve associated with the

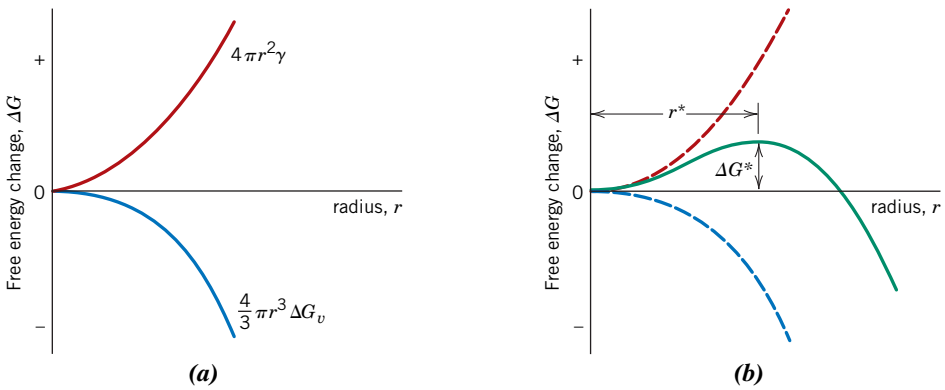

Figure 10.2 (*a*) Schematic curves for volume free energy and surface free energy contributions to the total free energy change attending the formation of a spherical embryo/nucleus during solidification. (*b*) Schematic plot of free energy versus embryo/nucleus radius, on which is shown the critical free energy change (ΔG^*) and the critical nucleus radius (r^*).

sum of both terms (Figure 10.2*b*) first increases, passes through a maximum, and finally decreases. In a physical sense, this means that as a solid particle begins to form as atoms in the liquid cluster together, its free energy first increases. If this cluster reaches a size corresponding to the critical radius r^*, then growth will continue with the accompaniment of a decrease in free energy. However, a cluster of radius less than the critical value will shrink and redissolve. This subcritical particle is an *embryo,* and the particle of radius greater than r^* is termed a *nucleus*. A critical free energy, ΔG^*, occurs at the critical radius and, consequently, at the maximum of the curve in Figure 10.2*b*. This ΔG^* corresponds to an *activation free energy,* which is the free energy required for the formation of a stable nucleus. Equivalently, it may be considered an energy barrier to the nucleation process.

Because r^* and ΔG^* appear at the maximum on the free energy-versus-radius curve of Figure 10.2*b*, derivation of expressions for these two parameters is a simple matter. For r^*, we differentiate the ΔG equation (Equation 10.1) with respect to r, set the resulting expression equal to zero, and then solve for r ($= r^*$). That is,

$$\frac{d(\Delta G)}{dr} = \tfrac{4}{3}\pi \Delta G_v(3r^2) + 4\pi\gamma(2r) = 0 \tag{10.2}$$

which leads to the result

For homogeneous nucleation, critical radius of a stable solid particle nucleus

$$r^* = -\frac{2\gamma}{\Delta G_v} \tag{10.3}$$

Now, substitution of this expression for r^* into Equation 10.1 yields the following expression for ΔG^*:

For homogeneous nucleation, activation free energy required for the formation of a stable nucleus

$$\Delta G^* = \frac{16\pi\gamma^3}{3(\Delta G_v)^2} \tag{10.4}$$

This volume free energy change ΔG_v is the driving force for the solidification transformation, and its magnitude is a function of temperature. At the equilibrium solidification temperature T_m, the value of ΔG_v is zero, and with decreasing temperature its value becomes increasingly more negative.

It can be shown that ΔG_v is a function of temperature as

$$\Delta G_v = \frac{\Delta H_f(T_m - T)}{T_m} \tag{10.5}$$

where ΔH_f is the latent heat of fusion (i.e., the heat given up during solidification), and T_m and the temperature T are in Kelvin. Substitution of this expression for ΔG_v into Equations 10.3 and 10.4 yields

Dependence of critical radius on surface free energy, latent heat of fusion, melting temperature, and transformation temperature

$$r^* = \left(-\frac{2\gamma T_m}{\Delta H_f}\right)\left(\frac{1}{T_m - T}\right) \tag{10.6}$$

and

Activation free energy expression

$$\Delta G^* = \left(\frac{16\pi\gamma^3 T_m^2}{3\Delta H_f^2}\right)\frac{1}{(T_m - T)^2} \tag{10.7}$$

Thus, from these two equations, both the critical radius r^* and the activation free energy ΔG^* decrease as temperature T decreases. (The γ and ΔH_f parameters in these

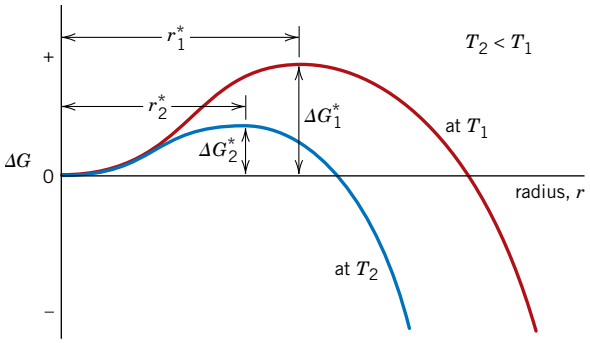

Figure 10.3 Schematic free energy-versus-embryo/nucleus-radius curves for two different temperatures. The critical free energy change (ΔG^*) and critical nucleus radius (r^*) are indicated for each temperature.

expressions are relatively insensitive to temperature changes.) Figure 10.3, a schematic ΔG-versus-r plot that shows curves for two different temperatures, illustrates these relationships. Physically, this means that with a lowering of temperature at temperatures below the equilibrium solidification temperature (T_m), nucleation occurs more readily. Furthermore, the number of stable nuclei n^* (having radii greater than r^*) is a function of temperature as

$$n^* = K_1 \exp\left(-\frac{\Delta G^*}{kT}\right) \tag{10.8}$$

where the constant K_1 is related to the total number of nuclei of the solid phase. For the exponential term of this expression, changes in temperature have a greater effect on the magnitude of the ΔG^* term in the numerator than the T term in the denominator. Consequently, as the temperature is lowered below T_m, the exponential term in Equation 10.8 also decreases, so that the magnitude of n^* increases. This temperature dependence (n^* versus T) is represented in the schematic plot of Figure 10.4*a*.

Another important temperature-dependent step is involved in and also influences nucleation: the clustering of atoms by short-range diffusion during the formation of nuclei. The influence of temperature on the rate of diffusion (i.e., magnitude of the diffusion coefficient, D) is given in Equation 5.8. Furthermore, this diffusion effect is related to the frequency at which atoms from the liquid attach themselves to the

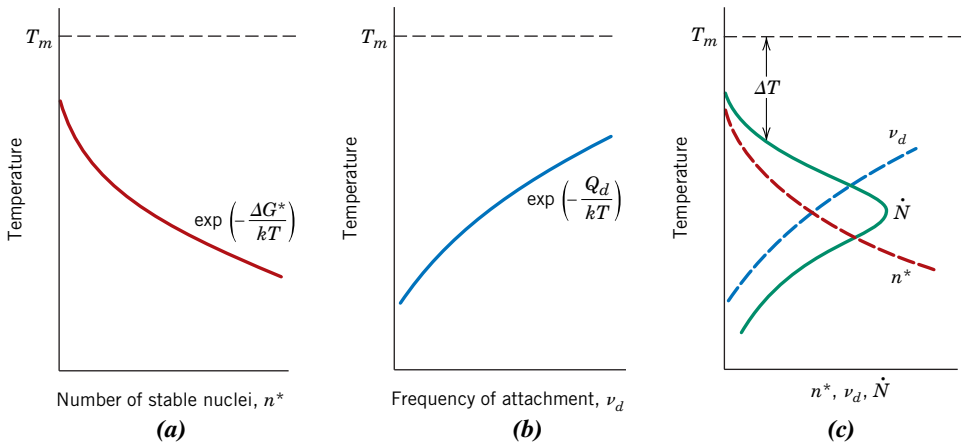

Figure 10.4 For solidification, schematic plots of (*a*) number of stable nuclei versus temperature, (*b*) frequency of atomic attachment versus temperature, and (*c*) nucleation rate versus temperature (the dashed curves are reproduced from parts *a* and *b*).

solid nucleus, v_d. The dependence of v_d on temperature is the same as for the diffusion coefficient—namely,

$$v_d = K_2 \exp\left(-\frac{Q_d}{kT}\right) \tag{10.9}$$

where Q_d is a temperature-independent parameter—the activation energy for diffusion—and K_2 is a temperature-independent constant. Thus, from Equation 10.9, a decrease of temperature results in a reduction in v_d. This effect, represented by the curve shown in Figure 10.4*b*, is just the reverse of that for n^* as discussed earlier.

The principles and concepts just developed are now extended to a discussion of another important nucleation parameter, the nucleation rate $\dot{N}$ (which has units of nuclei per unit volume per second). This rate is simply proportional to the product of n^* (Equation 10.8) and v_d (Equation 10.9)—that is,

Nucleation rate expression for homogeneous nucleation

$$\dot{N} = K_3 n^* v_d = K_1 K_2 K_3 \left[\exp\left(-\frac{\Delta G^*}{kT}\right)\exp\left(-\frac{Q_d}{kT}\right)\right] \tag{10.10}$$

Here, K_3 is the number of atoms on a nucleus surface. Figure 10.4*c* schematically plots nucleation rate as a function of temperature and, in addition, the curves of Figures 10.4*a* and 10.4*b* from which the $\dot{N}$ curve is derived. Figure 10.4*c* shows that, with a reduction of temperature from below T_m, the nucleation rate first increases, achieves a maximum, and subsequently diminishes.

The shape of this $\dot{N}$ curve is explained as follows: for the upper region of the curve (a sudden and dramatic increase in $\dot{N}$ with decreasing T), ΔG^* is greater than Q_d, which means that the $\exp(-\Delta G^*/kT)$ term of Equation 10.10 is much smaller than $\exp(-Q_d/kT)$. In other words, the nucleation rate is suppressed at high temperatures because of a small activation driving force. With continued reduction of temperature, there comes a point at which ΔG^* becomes smaller than the temperature-independent Q_d, with the result that $\exp(-Q_d/kT) < \exp(-\Delta G^*/kT)$, or that, at lower temperatures, a low atomic mobility suppresses the nucleation rate. This accounts for the shape of the lower curve segment (a precipitous reduction of $\dot{N}$ with a continued reduction of temperature). Furthermore, the $\dot{N}$ curve of Figure 10.4*c* necessarily passes through a maximum over the intermediate temperature range, where values for ΔG^* and Q_d are of approximately the same magnitude.

Several qualifying comments are in order regarding the preceding discussion. First, although we assumed a spherical shape for nuclei, this method may be applied to any shape with the same final result. Furthermore, this treatment may be used for types of transformations other than solidification (i.e., liquid–solid)—for example, solid–vapor and solid–solid. However, magnitudes of ΔG_v and γ, in addition to diffusion rates of the atomic species, will undoubtedly differ among the various transformation types. In addition, for solid–solid transformations, there may be volume changes attendant to the formation of new phases. These changes may lead to the introduction of microscopic strains, which must be taken into account in the ΔG expression of Equation 10.1 and, consequently, will affect the magnitudes of r^* and ΔG^*.

From Figure 10.4*c* it is apparent that during the cooling of a liquid, an appreciable nucleation rate (i.e., solidification) will begin only after the temperature has been lowered to below the equilibrium solidification (or melting) temperature (T_m). This phenomenon is termed *supercooling* (or *undercooling*), and the degree of supercooling for homogeneous nucleation may be significant (on the order of several hundred degrees Kelvin) for some systems. Table 10.1 shows, for several materials, typical degrees of supercooling for homogeneous nucleation.

Table 10.1
Degree of Supercooling (ΔT) Values (Homogeneous Nucleation) for Several Metals

Metal	ΔT (°C)
Antimony	135
Germanium	227
Silver	227
Gold	230
Copper	236
Iron	295
Nickel	319
Cobalt	330
Palladium	332

Source: D. Turnbull and R. E. Cech, "Microscopic Observation of the Solidification of Small Metal Droplets," *J. Appl. Phys.*, **21**, 808 (1950).

EXAMPLE PROBLEM 10.1

Computation of Critical Nucleus Radius and Activation Free Energy

(a) For the solidification of pure gold, calculate the critical radius r^* and the activation free energy ΔG^* if nucleation is homogeneous. Values for the latent heat of fusion and surface free energy are -1.16×10^9 J/m^3 and 0.132 J/m^2, respectively. Use the supercooling value in Table 10.1.

(b) Now, calculate the number of atoms found in a nucleus of critical size. Assume a lattice parameter of 0.413 nm for solid gold at its melting temperature.

Solution

(a) In order to compute the critical radius, we employ Equation 10.6, using the melting temperature of 1064°C for gold, assuming a supercooling value of 230°C (Table 10.1), and realizing that ΔH_f is negative. Hence

$$\begin{aligned} r^* &= \left(-\frac{2\gamma T_m}{\Delta H_f}\right)\left(\frac{1}{T_m - T}\right) \\ &= \left[-\frac{(2)(0.132\ \text{J/m}^2)(1064 + 273\ \text{K})}{-1.16 \times 10^9\ \text{J/m}^3}\right]\left(\frac{1}{230\ \text{K}}\right) \\ &= 1.32 \times 10^{-9}\ \text{m} = 1.32\ \text{nm} \end{aligned}$$

For computation of the activation free energy, Equation 10.7 is employed. Thus,

$$\begin{aligned} \Delta G^* &= \left(\frac{16\pi\gamma^3 T_m^2}{3\Delta H_f^2}\right)\frac{1}{(T_m - T)^2} \\ &= \left[\frac{(16)(\pi)(0.132\ \text{J/m}^2)^3(1064 + 273\ \text{K})^2}{(3)(-1.16 \times 10^9\ \text{J/m}^3)^2}\right]\left[\frac{1}{(230\ \text{K})^2}\right] \\ &= 9.64 \times 10^{-19}\ \text{J} \end{aligned}$$

(b) In order to compute the number of atoms in a nucleus of critical size (assuming a spherical nucleus of radius r^*), it is first necessary to determine the number of unit cells, which we then multiply by the number of atoms per unit cell. The number of unit cells found in this critical nucleus is just the ratio of critical nucleus and unit cell volumes. Inasmuch as gold has the FCC crystal structure (and a cubic unit cell), its unit cell volume is just a^3, where a is the lattice parameter (i.e., unit cell edge length); its value is 0.413 nm, as cited in the

problem statement. Therefore, the number of unit cells found in a radius of critical size is just

$$\#\text{ unit cells/particle} = \frac{\text{critical nucleus volume}}{\text{unit cell volume}} = \frac{\frac{4}{3}\pi r^{*3}}{a^3} \tag{10.11}$$

$$= \frac{\left(\frac{4}{3}\right)(\pi)(1.32\text{ nm})^3}{(0.413\text{ nm})^3} = 137\text{ unit cells}$$

Because of the equivalence of four atoms per FCC unit cell (Section 3.4), the total number of atoms per critical nucleus is just

(137 unit cells/critical nucleus)(4 atoms/unit cell) = 548 atoms/critical nucleus

Heterogeneous Nucleation

Although levels of supercooling for homogeneous nucleation may be significant (on occasion several hundred degrees Celsius), in practical situations they are often on the order of only several degrees Celsius. The reason for this is that the activation energy (i.e., energy barrier) for nucleation (ΔG^* of Equation 10.4) is lowered when nuclei form on preexisting surfaces or interfaces, because the surface free energy (γ of Equation 10.4) is reduced. In other words, it is easier for nucleation to occur at surfaces and interfaces than at other sites. Again, this type of nucleation is termed *heterogeneous*.

In order to understand this phenomenon, let us consider the nucleation, on a flat surface, of a solid particle from a liquid phase. It is assumed that both the liquid and solid phases "wet" this flat surface—that is, both of these phases spread out and cover the surface; this configuration is depicted schematically in Figure 10.5. Also noted in the figure are three interfacial energies (represented as vectors) that exist at two-phase boundaries—γ_{SL}, γ_{SI}, and γ_{IL}—as well as the wetting angle θ (the angle between the γ_{SI} and γ_{SL} vectors). Taking a surface tension force balance in the plane of the flat surface leads to the following expression:

For heterogeneous nucleation of a solid particle, relationship among solid–surface, solid–liquid, and liquid–surface interfacial energies and the wetting angle

$$\gamma_{IL} = \gamma_{SI} + \gamma_{SL}\cos\theta \tag{10.12}$$

Now, using a somewhat involved procedure similar to the one presented for homogeneous nucleation (which we have chosen to omit), it is possible to derive equations for r^* and ΔG^*; these are as follows:

For heterogeneous nucleation, critical radius of a stable solid particle nucleus

$$r^* = -\frac{2\gamma_{SL}}{\Delta G_v} \tag{10.13}$$

For heterogeneous nucleation, activation free energy required for the formation of a stable nucleus

$$\Delta G^* = \left(\frac{16\pi\gamma_{SL}^3}{3\Delta G_v^2}\right)S(\theta) \tag{10.14}$$

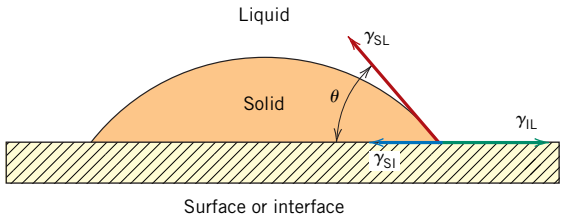

Figure 10.5 Heterogeneous nucleation of a solid from a liquid. The solid–surface (γ_{SI}), solid–liquid (γ_{SL}), and liquid–surface (γ_{IL}), interfacial energies are represented by vectors. The wetting angle (θ) is also shown.

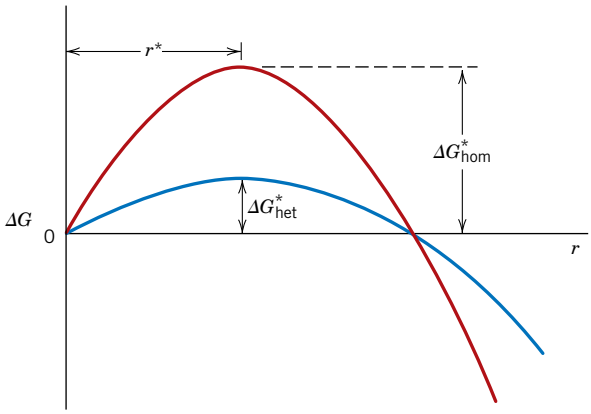

Figure 10.6 Schematic free-energy-versus-embryo/nucleus-radius plot on which are presented curves for both homogeneous and heterogeneous nucleation. Critical free energies and the critical radius are also shown.

The $S(\theta)$ term of this last equation is a function only of θ (i.e., the shape of the nucleus), which has a numerical value between zero and unity.[1]

From Equation 10.13, it is important to note that the critical radius r^* for heterogeneous nucleation is the same as for homogeneous nucleation, inasmuch as γ_{SL} is the same surface energy as γ in Equation 10.3. It is also evident that the activation energy barrier for heterogeneous nucleation (Equation 10.14) is smaller than the homogeneous barrier (Equation 10.4) by an amount corresponding to the value of this $S(\theta)$ function, or

$$\Delta G^*_{het} = \Delta G^*_{hom} S(\theta) \tag{10.15}$$

Figure 10.6, a schematic graph of ΔG versus nucleus radius, plots curves for both types of nucleation and indicates the difference in the magnitudes of ΔG^*_{het} and ΔG^*_{hom}, in addition to the constancy of r^*. This lower ΔG^* for heterogeneous nucleation means that a smaller energy must be overcome during the nucleation process (than for homogeneous nucleation), and, therefore, heterogeneous nucleation occurs more readily (Equation 10.10). In terms of the nucleation rate, the $\dot{N}$-versus-T curve (Figure 10.4*c*) is shifted to higher temperatures for heterogeneous. This effect is represented in Figure 10.7, which also shows that a much smaller degree of supercooling (ΔT) is required for heterogeneous nucleation.

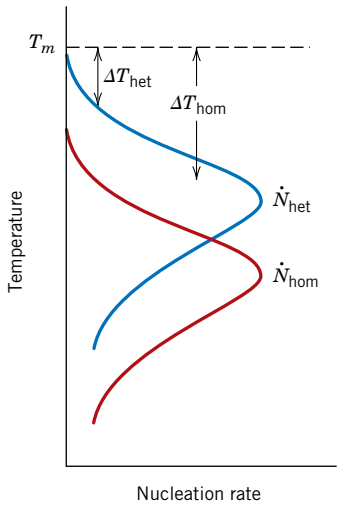

Figure 10.7 Nucleation rate versus temperature for both homogeneous and heterogeneous nucleation. Degree of supercooling (ΔT) for each is also shown.

[1]For example, for θ angles of 30° and 90°, values of $S(\theta)$ are approximately 0.01 and 0.5, respectively.

Growth

The growth step in a phase transformation begins once an embryo has exceeded the critical size, r^*, and becomes a stable nucleus. Note that nucleation will continue to occur simultaneously with growth of the new-phase particles; of course, nucleation cannot occur in regions that have already transformed into the new phase. Furthermore, the growth process will cease in any region where particles of the new phase meet because here the transformation will have reached completion.

Particle growth occurs by long-range atomic diffusion, which normally involves several steps—for example, diffusion through the parent phase, across a phase boundary, and then into the nucleus. Consequently, the growth rate $\dot{G}$ is determined by the rate of diffusion, and its temperature dependence is the same as for the diffusion coefficient (Equation 5.8)—namely,

Dependence of particle growth rate on the activation energy for diffusion and temperature

$$\dot{G} = C \exp\left(-\frac{Q}{kT}\right) \tag{10.16}$$

where Q (the activation energy) and C (a preexponential) are independent of temperature.[2] The temperature dependence of $\dot{G}$ is represented by one of the curves in Figure 10.8; also shown is a curve for the nucleation rate, $\dot{N}$ (again, almost always the rate for heterogeneous nucleation). Now, at a specific temperature, the overall transformation rate is equal to some product of $\dot{N}$ and $\dot{G}$. The third curve of Figure 10.8, which is for the total rate, represents this combined effect. The general shape of this curve is the same as for the nucleation rate, in that it has a peak or maximum that has been shifted upward relative to the $\dot{N}$ curve.

Whereas this treatment on transformations has been developed for solidification, the same general principles also apply to solid–solid and solid–gas transformations.

As we shall see later, the rate of transformation and the time required for the transformation to proceed to some degree of completion (e.g., time to 50% reaction completion, $t_{0.5}$) are inversely proportional to one another (Equation 10.18). Thus, if the logarithm of this transformation time (i.e., log $t_{0.5}$) is plotted versus temperature, a curve having the general shape shown in Figure 10.9*b* results. This "C-shaped" curve is a virtual mirror image (through a vertical plane) of the transformation rate curve of Figure 10.8, as demonstrated in Figure 10.9. The kinetics of phase transformations are often represented using logarithm time (to some degree of transformation) versus-temperature plots (for example, see Section 10.5).

Several physical phenomena may be explained in terms of the transformation rate–versus–temperature curve of Figure 10.8. First, the size of the product phase particles depends on transformation temperature. For example, for transformations that occur

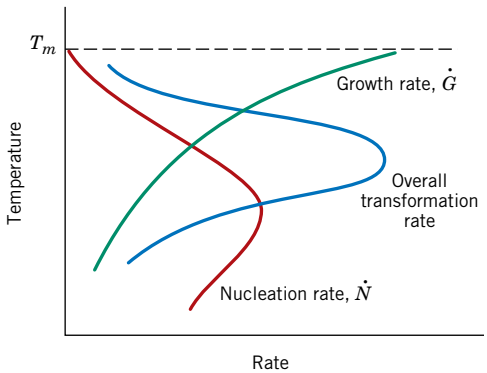

Figure 10.8 Schematic plot showing curves for nucleation rate ($\dot{N}$), growth rate ($\dot{G}$), and overall transformation rate versus temperature.

[2]Processes whose rates depend on temperature as $\dot{G}$ in Equation 10.16 are sometimes termed **thermally activated.** Also, a rate equation of this form (i.e., having the exponential temperature dependence) is termed an *Arrhenius rate equation*.

thermally activated transformation

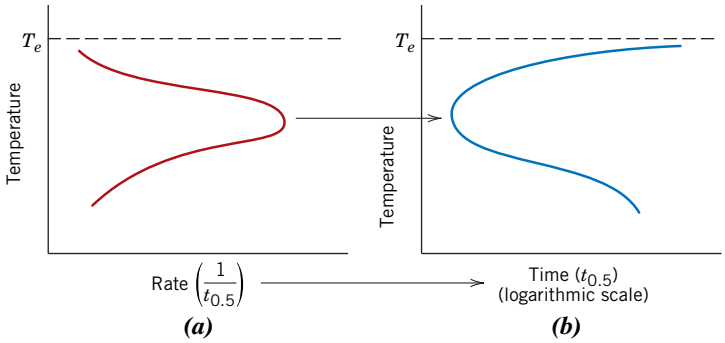

Figure 10.9 Schematic plots of (*a*) transformation rate versus temperature and (*b*) logarithm time [to some degree (e.g., 0.5 fraction) of transformation] versus temperature. The curves in both (*a*) and (*b*) are generated from the same set of data—that is, for horizontal axes, the time [scaled logarithmically in the (*b*) plot] is just the reciprocal of the rate from plot (*a*).

at temperatures near T_m, corresponding to low nucleation and high growth rates, few nuclei form that grow rapidly. Thus, the resulting microstructure will consist of few and relatively large particles (e.g., coarse grains). Conversely, for transformations at lower temperatures, nucleation rates are high and growth rates low, which results in many small particles (e.g., fine grains).

Also, from Figure 10.8, when a material is cooled very rapidly through the temperature range encompassed by the transformation rate curve to a relatively low temperature where the rate is extremely low, it is possible to produce nonequilibrium phase structures (e.g., see Sections 10.5 and 11.9).

Kinetic Considerations of Solid-State Transformations

kinetics

The previous discussion of this section centered on the temperature dependences of nucleation, growth, and transformation rates. The *time* dependence of rate (which is often termed the **kinetics** of a transformation) is also an important consideration, especially in the heat treatment of materials. Also, because many transformations of interest to materials scientists and engineers involve only solid phases, we devote the following discussion to the kinetics of solid-state transformations.

With many kinetic investigations, the fraction of reaction that has occurred is measured as a function of time while the temperature is maintained constant. Transformation progress is usually ascertained by either microscopic examination or measurement of some physical property (such as electrical conductivity) whose magnitude is distinctive of the new phase. Data are plotted as the fraction of transformed material versus the logarithm of time; an S-shaped curve similar to that in Figure 10.10 represents the typical kinetic behavior for most solid-state reactions. Nucleation and growth stages are also indicated in the figure.

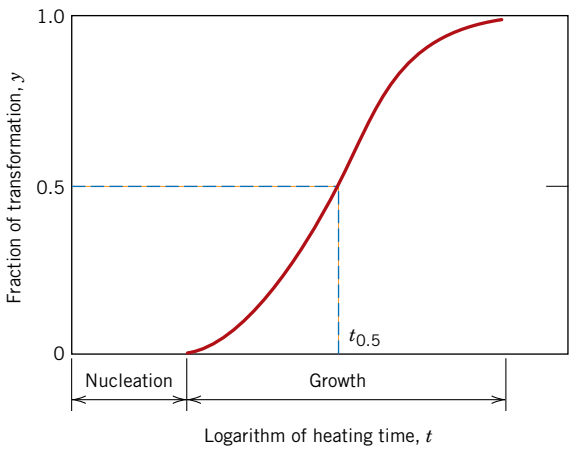

Figure 10.10 Plot of fraction reacted versus the logarithm of time typical of many solid-state transformations in which temperature is held constant.

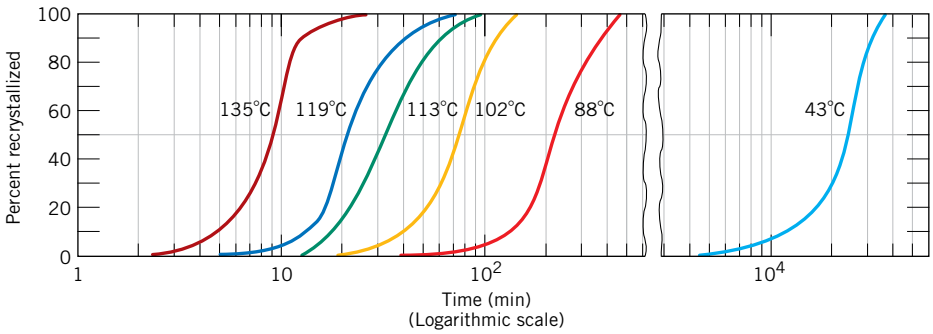

Figure 10.11 Percent recrystallization as a function of time and at constant temperature for pure copper. (Reprinted with permission from *Metallurgical Transactions,* Vol. 188, 1950, a publication of The Metallurgical Society of AIME, Warrendale, PA. Adapted from B. F. Decker and D. Harker, "Recrystallization in Rolled Copper," *Trans. AIME,* **188,** 1950, p. 888.)

Avrami equation—dependence of fraction of transformation on time

For solid-state transformations displaying the kinetic behavior in Figure 10.10, the fraction of transformation y is a function of time t as follows:

$$y = 1 - \exp(-kt^n) \tag{10.17}$$

where k and n are time-independent constants for the particular reaction. This expression is often referred to as the *Avrami equation*.

Transformation rate—reciprocal of the halfway-to-completion transformation time

By convention, the rate of a transformation is taken as the reciprocal of time required for the transformation to proceed halfway to completion, $t_{0.5}$, or

$$\text{rate} = \frac{1}{t_{0.5}} \tag{10.18}$$

Temperature has a profound influence on the kinetics and thus on the rate of a transformation. This is demonstrated in Figure 10.11, which shows y-versus-log$t$ S-shaped curves at several temperatures for the recrystallization of copper.

Section 10.5 gives a detailed discussion on the influence of both temperature and time on phase transformations.

EXAMPLE PROBLEM 10.2

Rate of Recrystallization Computation

It is known that the kinetics of recrystallization for some alloy obeys the Avrami equation and that the value of n is 3.1. If the fraction recrystallized is 0.30 after 20 min, determine the rate of recrystallization.

Solution

The rate of a reaction is defined by Equation 10.18 as

$$\text{rate} = \frac{1}{t_{0.5}}$$

Therefore, for this problem it is necessary to compute the value of $t_{0.5}$, the time it takes for the reaction to progress to 50% completion—or for the fraction of reaction y to equal 0.50. Furthermore, we may determine $t_{0.5}$ using the Avrami equation, Equation 10.17:

$$y = 1 - \exp(-kt^n)$$

The problem statement provides us with the value of y (0.30) at some time t (20 min), and also the value of n (3.1) from which data it is possible to compute the value of the constant k. In order to perform this calculation, some algebraic manipulation of Equation 10.17 is necessary. First, we rearrange this expression as follows:

$$\exp(-kt^n) = 1 - y$$

Taking natural logarithms of both sides leads to

$$-kt^n = \ln(1 - y) \tag{10.17a}$$

Now, solving for k,

$$k = -\frac{\ln(1 - y)}{t^n}$$

Incorporating values cited above for y, n, and t yields the following value for k:

$$k = -\frac{\ln(1 - 0.30)}{(20\ \text{min})^{3.1}} = 3.30 \times 10^{-5}$$

At this point, we want to compute $t_{0.5}$—the value of t for $y = 0.5$—which means that it is necessary to establish a form of Equation 10.17 in which t is the dependent variable. This is accomplished using a rearranged form of Equation 10.17a as

$$t^n = -\frac{\ln(1 - y)}{k}$$

From which we solve for t

$$t = \left[-\frac{\ln(1 - y)}{k}\right]^{1/n}$$

And for $t = t_{0.5}$, this equation becomes

$$t_{0.5} = \left[-\frac{\ln(1 - 0.5)}{k}\right]^{1/n}$$

Now, substituting into this expression the value of k determined above, as well as the value of n cited in the problem statement (viz., 3.1), we calculate $t_{0.5}$ as follows:

$$t_{0.5} = \left[-\frac{\ln(1 - 0.5)}{3.30 \times 10^{-5}}\right]^{1/3.1} = 24.8\ \text{min}$$

And, finally, from Equation 10.18, the rate is equal to

$$\text{rate} = \frac{1}{t_{0.5}} = \frac{1}{24.8\ \text{min}} = 4.0 \times 10^{-2}\ (\text{min})^{-1}$$

10.4 METASTABLE VERSUS EQUILIBRIUM STATES

Phase transformations may be wrought in metal alloy systems by varying temperature, composition, and the external pressure; however, temperature changes by means of heat treatments are most conveniently utilized to induce phase transformations. This corresponds to crossing a phase boundary on the composition–temperature phase diagram as an alloy of given composition is heated or cooled.

During a phase transformation, an alloy proceeds toward an equilibrium state that is characterized by the phase diagram in terms of the product phases and their compositions and relative amounts. As Section 10.3 notes, most phase transformations require some finite time to go to completion, and the speed or rate is often important in the relationship between the heat treatment and the development of microstructure. One limitation of phase diagrams is their inability to indicate the time period required for the attainment of equilibrium.

The rate of approach to equilibrium for solid systems is so slow that true equilibrium structures are rarely achieved. When phase transformations are induced by temperature changes, equilibrium conditions are maintained only if heating or cooling is carried out at extremely slow and unpractical rates. For other-than-equilibrium cooling, transformations are shifted to lower temperatures than indicated by the phase diagram; for heating, the shift is to higher temperatures. These phenomena are termed **supercooling** and **superheating,** respectively. The degree of each depends on the rate of temperature change; the more rapid the cooling or heating, the greater the supercooling or superheating. For example, for normal cooling rates, the iron–carbon eutectoid reaction is typically displaced 10°C to 20°C (18°F to 36°F) below the equilibrium transformation temperature.[3]

supercooling

superheating

For many technologically important alloys, the preferred state or microstructure is a metastable one, intermediate between the initial and equilibrium states; on occasion, a structure far removed from the equilibrium one is desired. It thus becomes imperative to investigate the influence of time on phase transformations. This kinetic information is, in many instances, of greater value than knowledge of the final equilibrium state.

Microstructural and Property Changes in Iron–Carbon Alloys

Some of the basic kinetic principles of solid-state transformations are now extended and applied specifically to iron–carbon alloys in terms of the relationships among heat treatment, the development of microstructure, and mechanical properties. This system has been chosen because it is familiar and because a wide variety of microstructures and mechanical properties is possible for iron–carbon (or steel) alloys.

10.5 ISOTHERMAL TRANSFORMATION DIAGRAMS

Pearlite

Consider again the iron–iron carbide eutectoid reaction

Eutectoid reaction for the iron–iron carbide system

$$\gamma(0.76\ \text{wt\%C}) \underset{\text{heating}}{\overset{\text{cooling}}{\rightleftharpoons}} \alpha(0.022\ \text{wt\% C}) + \text{Fe}_3\text{C}\ (6.70\ \text{wt\% C}) \tag{10.19}$$

which is fundamental to the development of microstructure in steel alloys. Upon cooling, austenite, having an intermediate carbon concentration, transforms into a ferrite phase, which has a much lower carbon content, and also cementite, which has a much higher carbon concentration. Pearlite is one microstructural product of this transformation (Figure 9.27); the mechanism of pearlite formation was discussed previously (Section 9.19) and demonstrated in Figure 9.28.

[3]It is important to note that the treatments relating to the kinetics of phase transformations in Section 10.3 are constrained to the condition of constant temperature. By way of contrast, the discussion of this section pertains to phase transformations that occur with changing temperature. This same distinction exists between Sections 10.5 (Isothermal Transformation Diagrams) and 10.6 (Continuous-Cooling Transformation Diagrams).

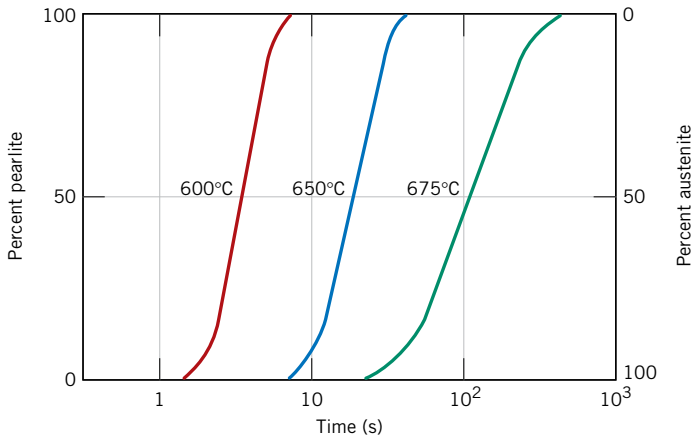

Figure 10.12 For an iron–carbon alloy of eutectoid composition (0.76 wt% C), isothermal fraction reacted versus the logarithm of time for the austenite-to-pearlite transformation.

Temperature plays an important role in the rate of the austenite-to-pearlite transformation. The temperature dependence for an iron–carbon alloy of eutectoid composition is indicated in Figure 10.12, which plots S-shaped curves of the percentage transformation versus the logarithm of time at three different temperatures. For each curve, data were collected after rapidly cooling a specimen composed of 100% austenite to the temperature indicated; that temperature was maintained constant throughout the course of the reaction.

A more convenient way of representing both the time and temperature dependence of this transformation is shown in the bottom portion of Figure 10.13. Here, the vertical and horizontal axes are, respectively, temperature and the logarithm of time. Two solid curves are plotted; one represents the time required at each temperature

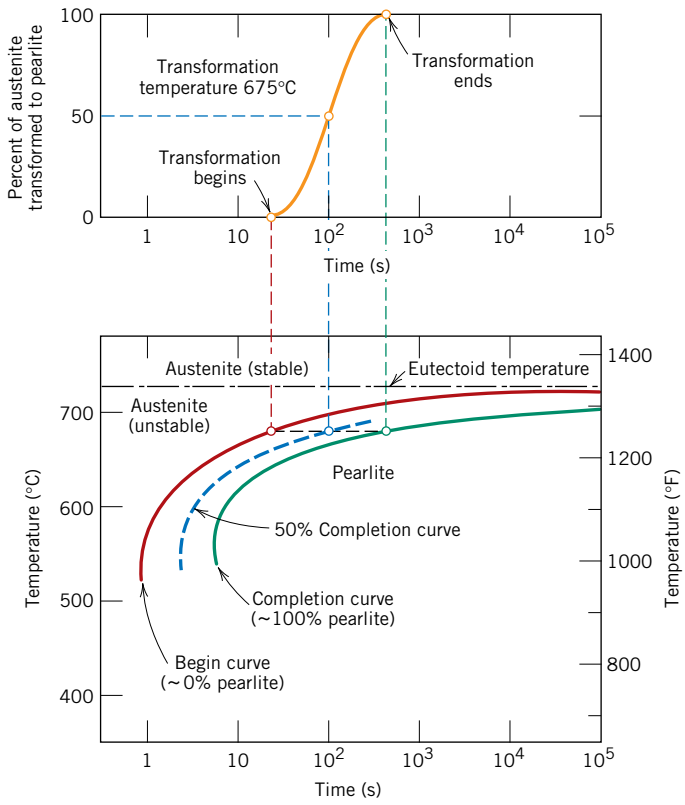

Figure 10.13 Demonstration of how an isothermal transformation diagram (bottom) is generated from percentage transformation-versus-logarithm of time measurements (top). [Adapted from H. Boyer (Editor), *Atlas of Isothermal Transformation and Cooling Transformation Diagrams,* 1977. Reproduced by permission of ASM International, Materials Park, OH.]

for the initiation or start of the transformation, and the other is for the transformation conclusion. The dashed curve corresponds to 50% of transformation completion. These curves were generated from a series of plots of the percentage transformation versus the logarithm of time taken over a range of temperatures. The S-shape curve [for 675°C (1247°F)] in the upper portion of Figure 10.13 illustrates how the data transfer is made.

In interpreting this diagram, note first that the eutectoid temperature [727°C (1341°F)] is indicated by a horizontal line; at temperatures above the eutectoid and for all times, only austenite exists, as indicated in the figure. The austenite-to-pearlite transformation occurs only if an alloy is supercooled to below the eutectoid; as indicated by the curves, the time necessary for the transformation to begin and then end depends on temperature. The start and finish curves are nearly parallel, and they approach the eutectoid line asymptotically. To the left of the transformation start curve, only austenite (which is unstable) is present, whereas to the right of the finish curve, only pearlite exists. In between, the austenite is in the process of transforming to pearlite, and thus both microconstituents are present.

According to Equation 10.18, the transformation rate at some particular temperature is inversely proportional to the time required for the reaction to proceed to 50% completion (to the dashed line in Figure 10.13). That is, the shorter this time, the higher is the rate. Thus, from Figure 10.13, at temperatures just below the eutectoid (corresponding to just a slight degree of undercooling) very long times (on the order of 10^5 s) are required for the 50% transformation, and therefore the reaction rate is very slow. The transformation rate increases with decreasing temperature such that at 540°C (1000°F), only about 3 s is required for the reaction to go to 50% completion.

Several constraints are imposed on the use of diagrams like Figure 10.13. First, this particular plot is valid only for an iron–carbon alloy of eutectoid composition; for other compositions, the curves have different configurations. In addition, these plots are accurate only for transformations in which the temperature of the alloy is held constant throughout the duration of the reaction. Conditions of constant temperature are termed *isothermal;* thus, plots such as Figure 10.13 are referred to as **isothermal transformation diagrams** or sometimes as *time-temperature-transformation* (or *T-T-T*) plots.

isothermal transformation diagram

An actual isothermal heat treatment curve (*ABCD*) is superimposed on the isothermal transformation diagram for a eutectoid iron–carbon alloy in Figure 10.14. Very rapid cooling of austenite to a given temperature is indicated by the near-vertical line *AB*, and the isothermal treatment at this temperature is represented by the horizontal segment *BCD*. Time increases from left to right along this line. The transformation of austenite to pearlite begins at the intersection, point *C* (after approximately 3.5 s), and has reached completion by about 15 s, corresponding to point *D*. Figure 10.14 also shows schematic microstructures at various times during the progression of the reaction.

The thickness ratio of the ferrite and cementite layers in pearlite is approximately 8 to 1. However, the absolute layer thickness depends on the temperature at which the isothermal transformation is allowed to occur. At temperatures just below the eutectoid, relatively thick layers of both the α-ferrite and Fe_3C phases are produced; this microstructure is called **coarse pearlite,** and the region at which it forms is indicated to the right of the completion curve on Figure 10.14. At these temperatures, diffusion rates are relatively high, such that during the transformation illustrated in Figure 9.28 carbon atoms can diffuse relatively long distances, which results in the formation of thick lamellae. With decreasing temperature, the carbon diffusion rate decreases, and the layers become progressively thinner. The thin-layered structure produced in the vicinity of 540°C is termed **fine pearlite;** this is also indicated in Figure 10.14. To be discussed in Section 10.7 is the dependence of mechanical properties on lamellar thickness. Photomicrographs of coarse and fine pearlite for a eutectoid composition are shown in Figure 10.15.

coarse pearlite

fine pearlite

For iron–carbon alloys of other compositions, a proeutectoid phase (either ferrite or cementite) coexists with pearlite, as discussed in Section 9.19. Thus, additional

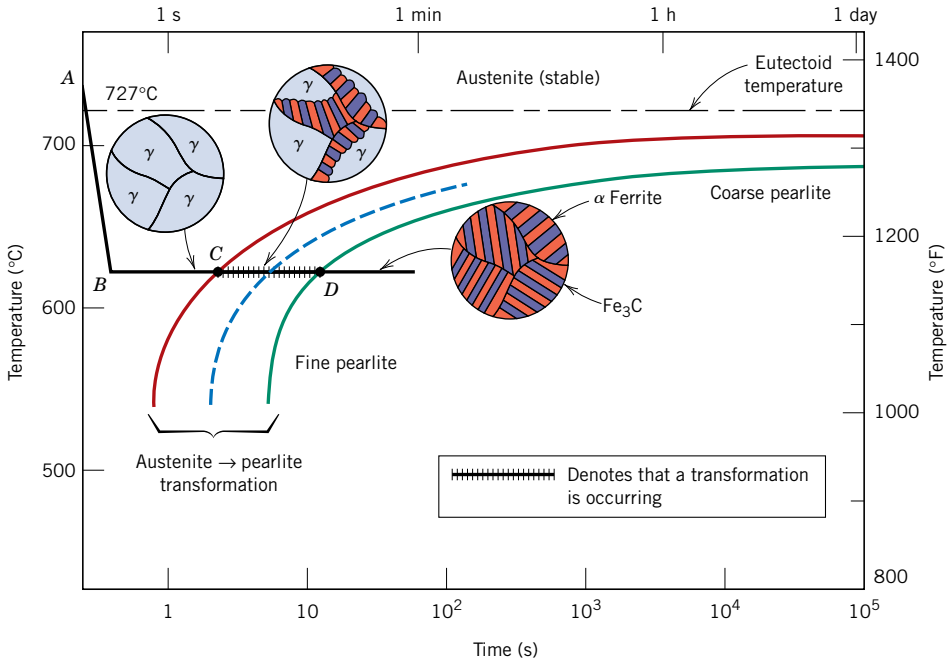

Figure 10.14 Isothermal transformation diagram for a eutectoid iron–carbon alloy, with superimposed isothermal heat treatment curve (*ABCD*). Microstructures before, during, and after the austenite-to-pearlite transformation are shown.
[Adapted from H. Boyer (Editor), *Atlas of Isothermal Transformation and Cooling Transformation Diagrams,* 1977. Reproduced by permission of ASM International, Materials Park, OH.]

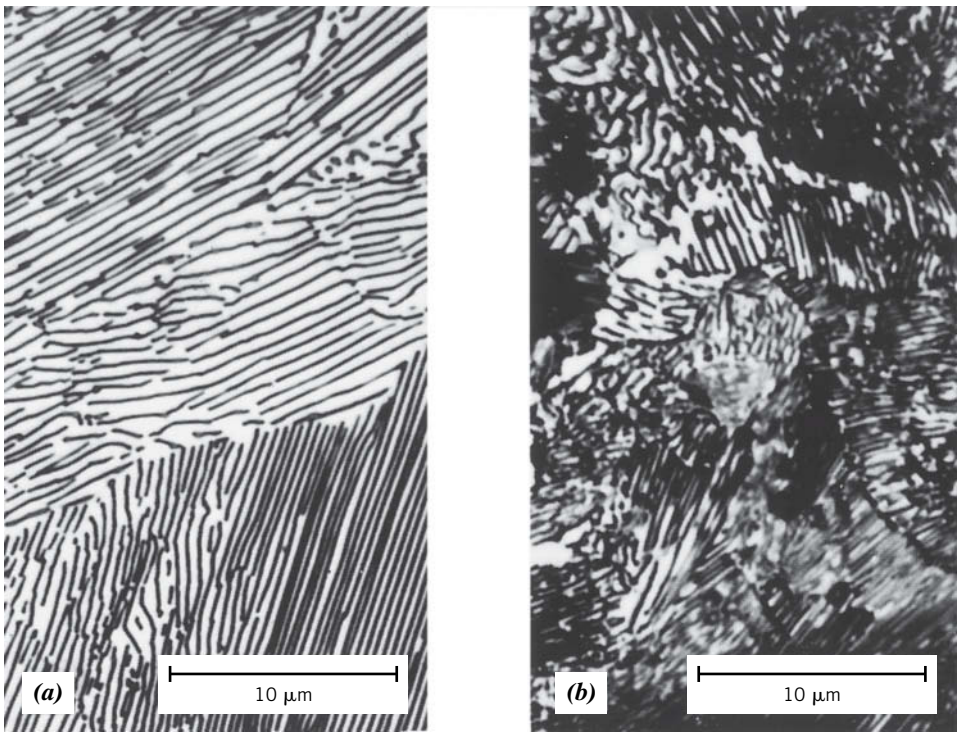

Figure 10.15 Photomicrographs of (*a*) coarse pearlite and (*b*) fine pearlite. 3000×.
(From K. M. Ralls et al., *An Introduction to Materials Science and Engineering*, p. 361. Copyright © 1976 by John Wiley & Sons, New York. Reprinted by permission of John Wiley & Sons, Inc.)

WileyPLUS

Tutorial Video: Iron–Carbon Alloy Microstructures
What is the Appearance of the Various Iron–Carbon Alloys and How Can I Draw Them?

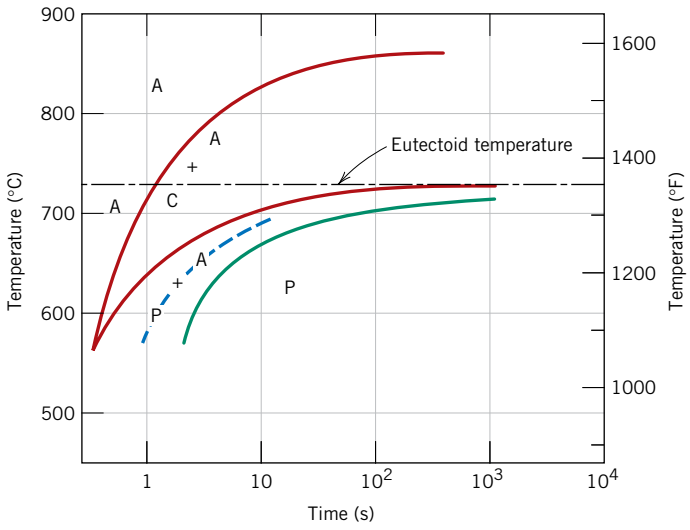

Figure 10.16 Isothermal transformation diagram for a 1.13 wt% C iron–carbon alloy: A, austenite; C, proeutectoid cementite; P, pearlite.
[Adapted from H. Boyer (Editor), *Atlas of Isothermal Transformation and Cooling Transformation Diagrams,* 1977. Reproduced by permission of ASM International, Materials Park, OH.]

curves corresponding to a proeutectoid transformation also must be included on the isothermal transformation diagram. A portion of one such diagram for a 1.13 wt% C alloy is shown in Figure 10.16.

Bainite

bainite

In addition to pearlite, other microconstituents that are products of the austenitic transformation exist; one of these is called **bainite.** The microstructure of bainite consists of ferrite and cementite phases, and thus diffusional processes are involved in its formation. Bainite forms as needles or plates, depending on the temperature of the transformation; the microstructural details of bainite are so fine that their resolution is possible only using electron microscopy. Figure 10.17 is an electron micrograph that shows a grain of bainite (positioned diagonally from lower left to upper right). It is composed of a ferrite matrix and elongated particles of Fe_3C; the various phases in this micrograph have been labeled.

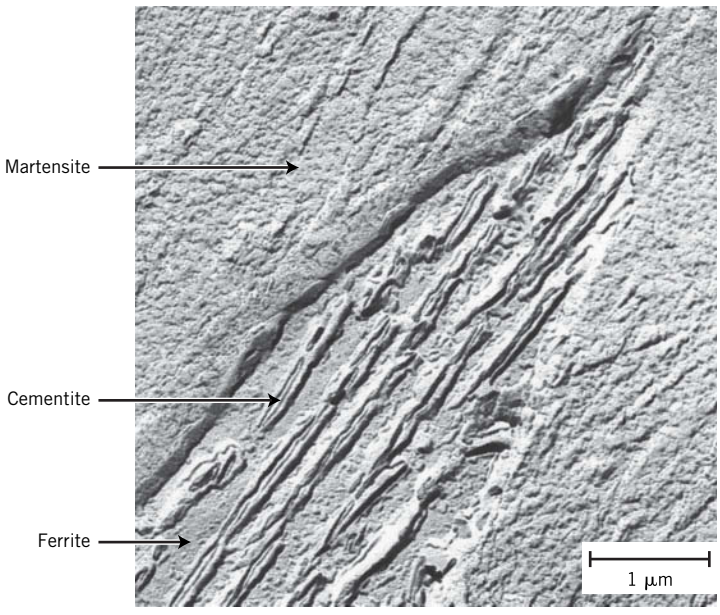

Figure 10.17 Transmission electron micrograph showing the structure of bainite. A grain of bainite passes from lower left to upper right corners; it consists of elongated and needle-shape particles of Fe_3C within a ferrite matrix. The phase surrounding the bainite is martensite.
(From *Metals Handbook,* Vol. 8, 8th edition, *Metallography, Structures and Phase Diagrams,* 1973. Reproduced by permission of ASM International, Materials Park, OH.)

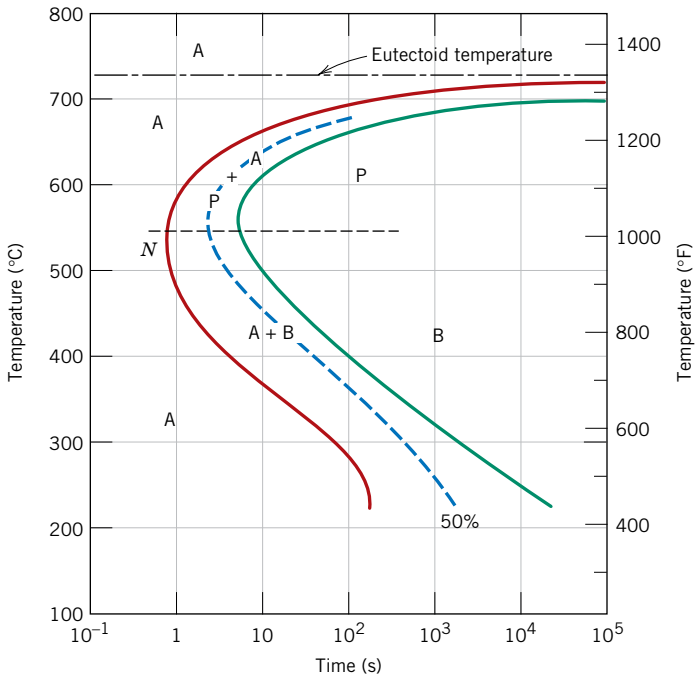

Figure 10.18 Isothermal transformation diagram for an iron–carbon alloy of eutectoid composition, including austenite-to-pearlite (A–P) and austenite-to-bainite (A–B) transformations.
[Adapted from H. Boyer (Editor), *Atlas of Isothermal Transformation and Cooling Transformation Diagrams,* 1977. Reproduced by permission of ASM International, Materials Park, OH.]

WileyPLUS

Tutorial Video: Isothermal Transformation Diagrams
How do I Read a TTT Diagram?

In addition, the phase that surrounds the needle is martensite, the topic addressed by a subsequent section. Furthermore, no proeutectoid phase forms with bainite.

The time–temperature dependence of the bainite transformation may also be represented on the isothermal transformation diagram. It occurs at temperatures below those at which pearlite forms; begin-, end-, and half-reaction curves are just extensions of those for the pearlitic transformation, as shown in Figure 10.18, the isothermal transformation diagram for an iron–carbon alloy of eutectoid composition that has been extended to lower temperatures. All three curves are C-shaped and have a "nose" at point *N*, where the rate of transformation is a maximum. As may be noted, whereas pearlite forms above the nose [i.e., over the temperature range of about 540°C to 727°C (1000°F to 1341°F)], at temperatures between about 215°C and 540°C (420°F and 1000°F), bainite is the transformation product.

Note that the pearlitic and bainitic transformations are competitive with each other, and once some portion of an alloy has transformed into either pearlite or bainite, transformation to the other microconstituent is not possible without reheating to form austenite.

Spheroidite

If a steel alloy having either pearlitic or bainitic microstructures is heated to, and left at, a temperature below the eutectoid for a sufficiently long period of time—for example, at about 700°C (1300°F) for between 18 and 24 h—yet another microstructure will form called **spheroidite** (Figure 10.19). Instead of the alternating ferrite and cementite lamellae (pearlite) or the microstructure observed for bainite, the Fe_3C phase appears as spherelike particles embedded in a continuous α–phase matrix. This transformation occurs by additional carbon diffusion with no change in the compositions or relative amounts of ferrite and cementite phases. The driving force for this transformation is the reduction in α–Fe_3C phase boundary area. The kinetics of spheroidite formation is not included on isothermal transformation diagrams.

spheroidite

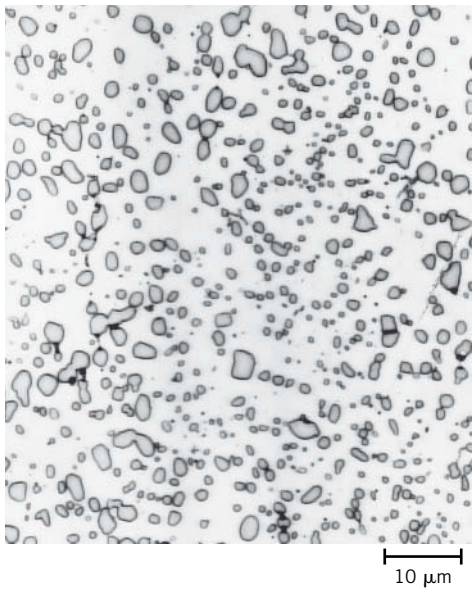

Figure 10.19 Photomicrograph of a steel having a spheroidite microstructure. The small particles are cementite; the continuous phase is α-ferrite. 1000×.
(Copyright 1971 by United States Steel Corporation.)

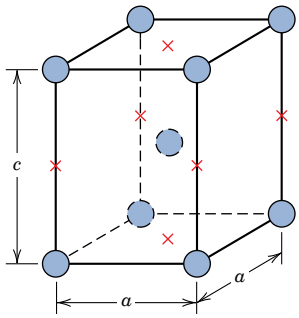

Figure 10.20 The body-centered tetragonal unit cell for martensitic steel showing iron atoms (circles) and sites that may be occupied by carbon atoms (×s). For this tetragonal unit cell, $c > a$.

Concept Check 10.1 Which is more stable, the pearlitic or the spheroiditic microstructure? Why?

[*The answer may be found at www.wiley.com/college/callister (Student Companion Site).*]

Martensite

martensite

Yet another microconstituent or phase called **martensite** is formed when austenitized iron–carbon alloys are rapidly cooled (or quenched) to a relatively low temperature (in the vicinity of the ambient). Martensite is a nonequilibrium single-phase structure that results from a diffusionless transformation of austenite. It may be thought of as a transformation product that is competitive with pearlite and bainite. The martensitic transformation occurs when the quenching rate is rapid enough to prevent carbon diffusion. Any diffusion whatsoever results in the formation of ferrite and cementite phases.

The martensitic transformation is not well understood. However, large numbers of atoms experience cooperative movements, in that there is only a slight displacement of each atom relative to its neighbors. This occurs in such a way that the FCC austenite experiences a polymorphic transformation to a body-centered tetragonal (BCT) martensite. A unit cell of this crystal structure (Figure 10.20) is simply a body-centered cube that has been elongated along one of its dimensions; this structure is distinctly different from that for BCC ferrite. All the carbon atoms remain as interstitial impurities in martensite; as such, they constitute a supersaturated solid solution that is capable of rapidly transforming to other structures if heated to temperatures at which diffusion rates become

Figure 10.21 Photomicrograph showing the martensitic microstructure. The needle-shape grains are the martensite phase, and the white regions are austenite that failed to transform during the rapid quench. 1220×.
(Photomicrograph courtesy of United States Steel Corporation.)

appreciable. Many steels, however, retain their martensitic structure almost indefinitely at room temperature.

The martensitic transformation is not, however, unique to iron–carbon alloys. It is found in other systems and is characterized, in part, by the diffusionless transformation.

Because the martensitic transformation does not involve diffusion, it occurs almost instantaneously; the martensite grains nucleate and grow at a very rapid rate—the velocity of sound within the austenite matrix. Thus the martensitic transformation rate, for all practical purposes, is time independent.

Martensite grains take on a platelike or needlelike appearance, as indicated in Figure 10.21. The white phase in the micrograph is austenite (retained austenite) that did not transform during the rapid quench. As already mentioned, martensite as well as other microconstituents (e.g., pearlite) can coexist.

Being a nonequilibrium phase, martensite does not appear on the iron–iron carbide phase diagram (Figure 9.24). The austenite-to-martensite transformation, however, is represented on the isothermal transformation diagram. Because the martensitic transformation is diffusionless and instantaneous, it is not depicted in this diagram as the pearlitic and bainitic reactions are. The beginning of this transformation is represented by a horizontal line designated M(start) (Figure 10.22). Two other horizontal and dashed lines, labeled M(50%) and M(90%), indicate percentages of the austenite-to-martensite transformation. The temperatures at which these lines are located vary with alloy composition, but they must be relatively low because carbon diffusion must be virtually nonexistent.[4] The horizontal and linear character of these lines indicates that the martensitic transformation is independent of time; it is a function only of the temperature to which the alloy is quenched or rapidly cooled. A transformation of this type is termed an **athermal transformation.**

athermal transformation

[4] The alloy that is the subject of Figure 10.21 is not an iron–carbon alloy of eutectoid composition; furthermore, its 100% martensite transformation temperature lies below room temperature. Because the photomicrograph was taken at room temperature, some austenite (i.e., the retained austenite) is present, having not transformed to martensite.

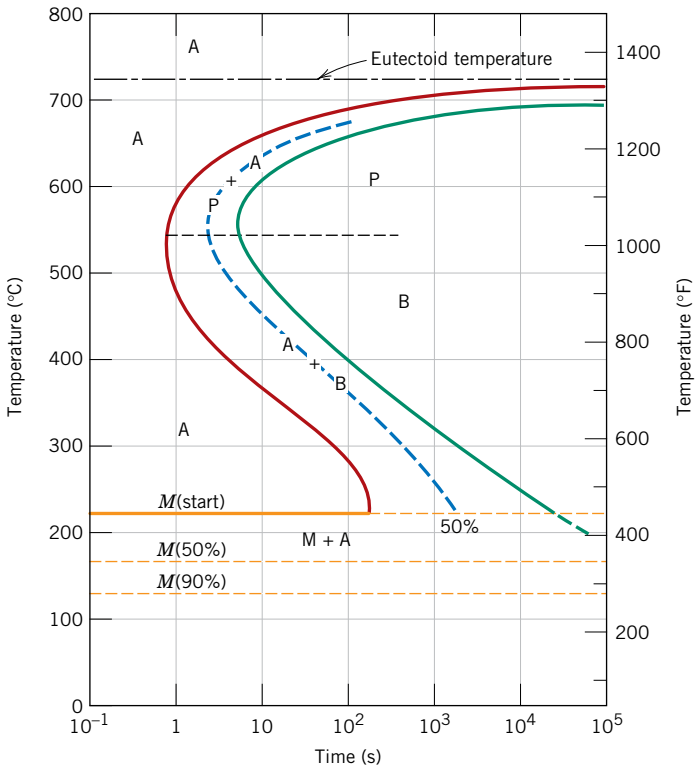

Figure 10.22 The complete isothermal transformation diagram for an iron–carbon alloy of eutectoid composition: A, austenite; B, bainite; M, martensite; P, pearlite.

Consider an alloy of eutectoid composition that is very rapidly cooled from a temperature above 727°C (1341°F) to, say, 165°C (330°F). From the isothermal transformation diagram (Figure 10.22) it may be noted that 50% of the austenite will immediately transform into martensite; as long as this temperature is maintained, there will be no further transformation.

The presence of alloying elements other than carbon (e.g., Cr, Ni, Mo, and W) may cause significant changes in the positions and shapes of the curves in the isothermal transformation diagrams. These include (1) shifting to longer times the nose of the austenite-to-pearlite transformation (and also a proeutectoid phase nose, if such exists), and (2) the formation of a separate bainite nose. These alterations may be observed by comparing Figures 10.22 and 10.23, which are isothermal transformation diagrams for carbon and alloy steels, respectively.

plain carbon steel

alloy steel

Steels in which carbon is the prime alloying element are termed **plain carbon steels**, whereas **alloy steels** contain appreciable concentrations of other elements, including those cited in the preceding paragraph. Section 11.2 discusses further the classification and properties of ferrous alloys.

Concept Check 10.2 Cite two major differences between martensitic and pearlitic transformations.

[*The answer may be found at www.wiley.com/college/callister (Student Companion Site).*]

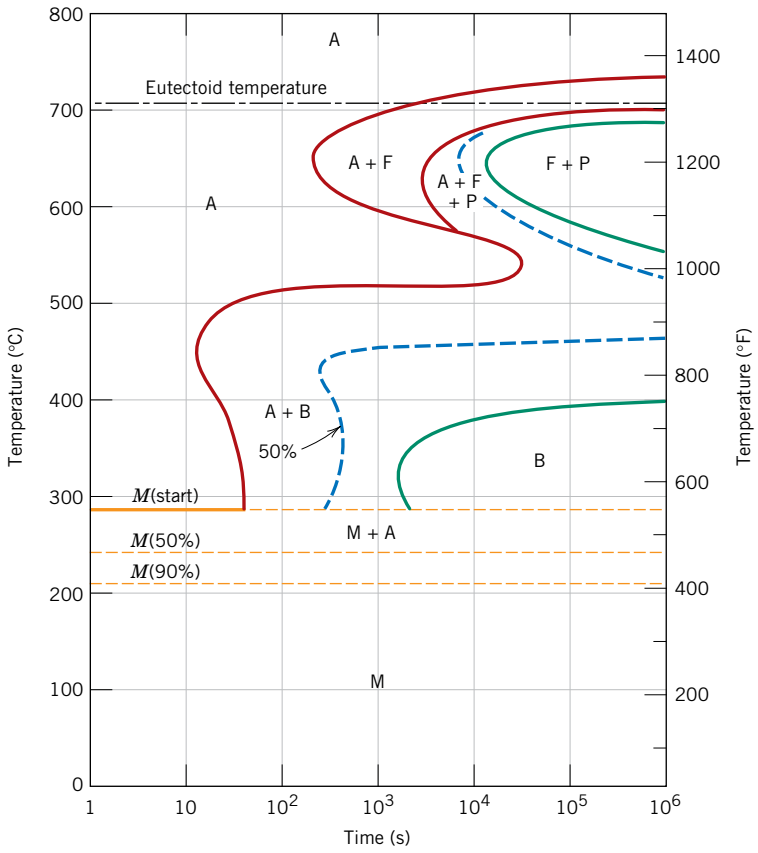

Figure 10.23 Isothermal transformation diagram for an alloy steel (type 4340): A, austenite; B, bainite; P, pearlite; M, martensite; F, proeutectoid ferrite.
[Adapted from H. Boyer (Editor), *Atlas of Isothermal Transformation and Cooling Transformation Diagrams,* 1977. Reproduced by permission of ASM International, Materials Park, OH.]

EXAMPLE PROBLEM 10.3

Microstructural Determinations for Three Isothermal Heat Treatments

Using the isothermal transformation diagram for an iron–carbon alloy of eutectoid composition (Figure 10.22), specify the nature of the final microstructure (in terms of microconstituents present and approximate percentages) of a small specimen that has been subjected to the following time–temperature treatments. In each case, assume that the specimen begins at 760°C (1400°F) and that it has been held at this temperature long enough to have achieved a complete and homogeneous austenitic structure.

WileyPLUS

Tutorial Video: Isothermal Transformation Diagrams
Which Heat Treatment Goes with Which Microstructure?

(a) Rapidly cool to 350°C (660°F), hold for 10^4 s, and quench to room temperature.
(b) Rapidly cool to 250°C (480°F), hold for 100 s, and quench to room temperature.
(c) Rapidly cool to 650°C (1200°F), hold for 20 s, rapidly cool to 400°C (750°F), hold for 10^3 s, and quench to room temperature.

Solution

The time–temperature paths for all three treatments are shown in Figure 10.24. In each case, the initial cooling is rapid enough to prevent any transformation from occurring.

(a) At 350°C austenite isothermally transforms into bainite; this reaction begins after about 10 s and reaches completion at about 500 s elapsed time. Therefore, by 10^4 s, as stipulated in this problem, 100% of the specimen is bainite, and no further transformation is

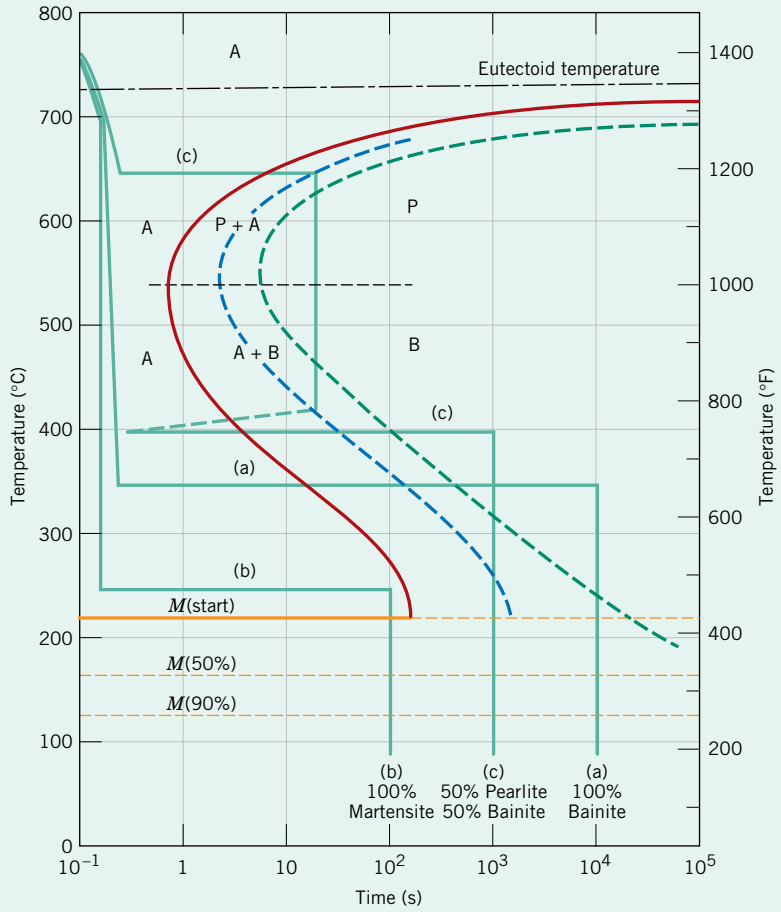

Figure 10.24 Isothermal transformation diagram for an iron–carbon alloy of eutectoid composition and the isothermal heat treatments (a), (b), and (c) in Example Problem 10.3.

possible, even though the final quenching line passes through the martensite region of the diagram.

(b) In this case, it takes about 150 s at 250°C for the bainite transformation to begin, so that at 100 s the specimen is still 100% austenite. As the specimen is cooled through the martensite region, beginning at about 215°C, progressively more of the austenite instantaneously transforms into martensite. This transformation is complete by the time room temperature is reached, such that the final microstructure is 100% martensite.

(c) For the isothermal line at 650°C, pearlite begins to form after about 7 s; by the time 20 s has elapsed, only approximately 50% of the specimen has transformed to pearlite. The rapid cool to 400°C is indicated by the vertical line; during this cooling, very little, if any, remaining austenite will transform to either pearlite or bainite, even though the cooling line passes through pearlite and bainite regions of the diagram. At 400°C, we begin timing at essentially zero time (as indicated in Figure 10.24); thus, by the time 10^3 s has elapsed, all of the remaining 50% austenite will have completely transformed to bainite. Upon quenching to room temperature, any further transformation is not possible inasmuch as no austenite remains, and so the final microstructure at room temperature consists of 50% pearlite and 50% bainite.

Concept Check 10.3 Make a copy of the isothermal transformation diagram for an iron–carbon alloy of eutectoid composition (Figure 10.22) and then sketch and label on this diagram a time–temperature path that will produce 100% fine pearlite.

[*The answer may be found at www.wiley.com/college/callister (Student Companion Site).*]

10.6 CONTINUOUS-COOLING TRANSFORMATION DIAGRAMS

Isothermal heat treatments are not the most practical to conduct because an alloy must be rapidly cooled to and maintained at an elevated temperature from a higher temperature above the eutectoid. Most heat treatments for steels involve the continuous cooling of a specimen to room temperature. An isothermal transformation diagram is valid only for conditions of constant temperature; this diagram must be modified for transformations that occur as the temperature is constantly changing. For continuous cooling, the time required for a reaction to begin and end is delayed. Thus the isothermal curves are shifted to longer times and lower temperatures, as indicated in Figure 10.25 for an iron–carbon alloy of eutectoid composition. A plot containing such modified beginning and ending reaction curves is termed a **continuous-cooling transformation** (*CCT*) **diagram.** Some control may be maintained over the rate of temperature change, depending on the cooling environment. Two cooling curves corresponding to moderately fast and

continuous-cooling transformation diagram

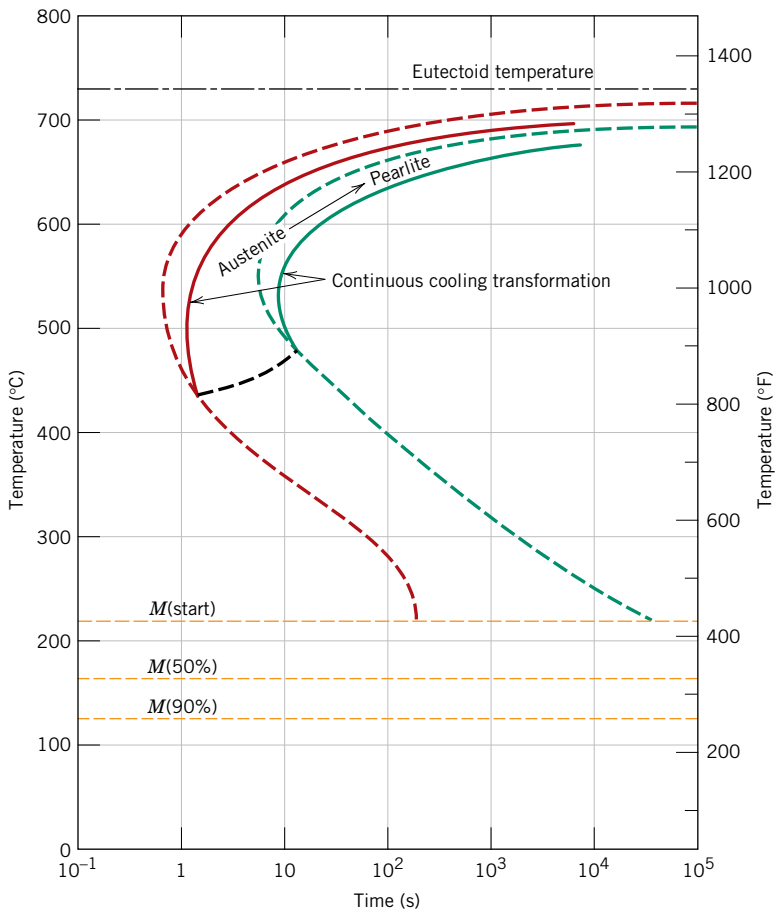

Figure 10.25 Superimposition of isothermal and continuous-cooling transformation diagrams for a eutectoid iron–carbon alloy.
[Adapted from H. Boyer (Editor), *Atlas of Isothermal Transformation and Cooling Transformation Diagrams,* 1977. Reproduced by permission of ASM International, Materials Park, OH.]

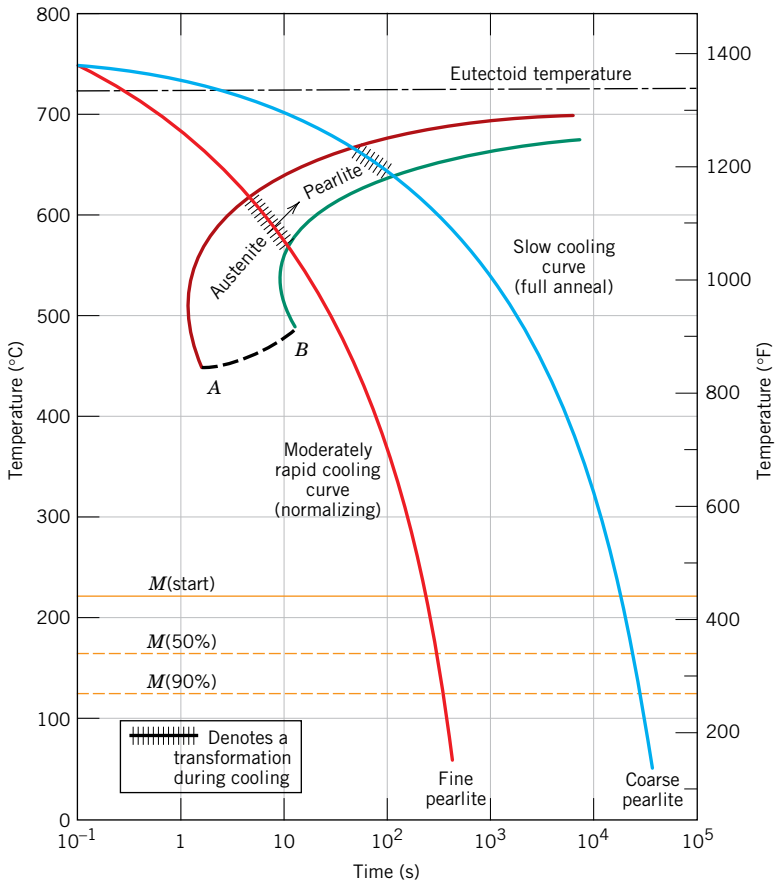

Figure 10.26 Moderately rapid and slow cooling curves superimposed on a continuous-cooling transformation diagram for a eutectoid iron–carbon alloy.

slow rates are superimposed and labeled in Figure 10.26, again for a eutectoid steel. The transformation starts after a time period corresponding to the intersection of the cooling curve with the beginning reaction curve and concludes upon crossing the completion transformation curve. The microstructural products for the moderately rapid and slow cooling rate curves in Figure 10.26 are fine and coarse pearlite, respectively.

Normally, bainite will not form when an alloy of eutectoid composition or, for that matter, any plain carbon steel is continuously cooled to room temperature. This is because all of the austenite has transformed into pearlite by the time the bainite transformation has become possible. Thus, the region representing the austenite–pearlite transformation terminates just below the nose (Figure 10.26), as indicated by the curve AB. For any cooling curve passing through AB in Figure 10.26, the transformation ceases at the point of intersection; with continued cooling, the unreacted austenite begins transforming into martensite upon crossing the M(start) line.

With regard to the representation of the martensitic transformation, the M(start), M(50%), and M(90%) lines occur at identical temperatures for both isothermal and continuous-cooling transformation diagrams. This may be verified for an iron–carbon alloy of eutectoid composition by comparison of Figures 10.22 and 10.25.

For the continuous cooling of a steel alloy, there exists a critical quenching rate, which represents the minimum rate of quenching that produces a totally martensitic structure. This critical cooling rate, when included on the continuous transformation diagram, just misses the nose at which the pearlite transformation begins, as illustrated in

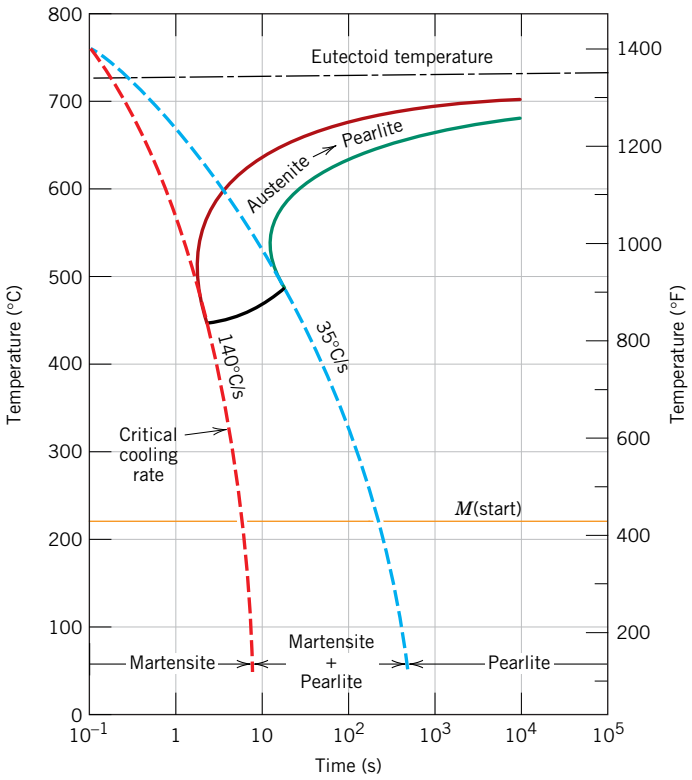

Figure 10.27 Continuous-cooling transformation diagram for a eutectoid iron–carbon alloy and superimposed cooling curves, demonstrating the dependence of the final microstructure on the transformations that occur during cooling.

Figure 10.27. As the figure also shows, only martensite exists for quenching rates greater than the critical one; in addition, there is a range of rates over which both pearlite and martensite are produced. Finally, a totally pearlitic structure develops for low cooling rates.

Carbon and other alloying elements also shift the pearlite (as well as the proeutectoid phase) and bainite noses to longer times, thus decreasing the critical cooling rate. In fact, one of the reasons for alloying steels is to facilitate the formation of martensite so that totally martensitic structures can develop in relatively thick cross sections. Figure 10.28 shows the continuous-cooling transformation diagram for the same alloy steel for which the isothermal transformation diagram is presented in Figure 10.23. The presence of the bainite nose accounts for the possibility of formation of bainite for a continuous-cooling heat treatment. Several cooling curves superimposed on Figure 10.28 indicate the critical cooling rate, and also how the transformation behavior and final microstructure are influenced by the rate of cooling.

Of interest, the critical cooling rate is decreased even by the presence of carbon. In fact, iron–carbon alloys containing less than about 0.25 wt% carbon are not normally heat-treated to form martensite because quenching rates too rapid to be practical are required. Other alloying elements that are particularly effective in rendering steels heat-treatable are chromium, nickel, molybdenum, manganese, silicon, and tungsten; however, these elements must be in solid solution with the austenite at the time of quenching.

In summary, isothermal and continuous-cooling transformation diagrams are, in a sense, phase diagrams in which the parameter of time is introduced. Each is experimentally determined for an alloy of specified composition, the variables being temperature and time. These diagrams allow prediction of the microstructure after some time period for constant-temperature and continuous-cooling heat treatments, respectively.

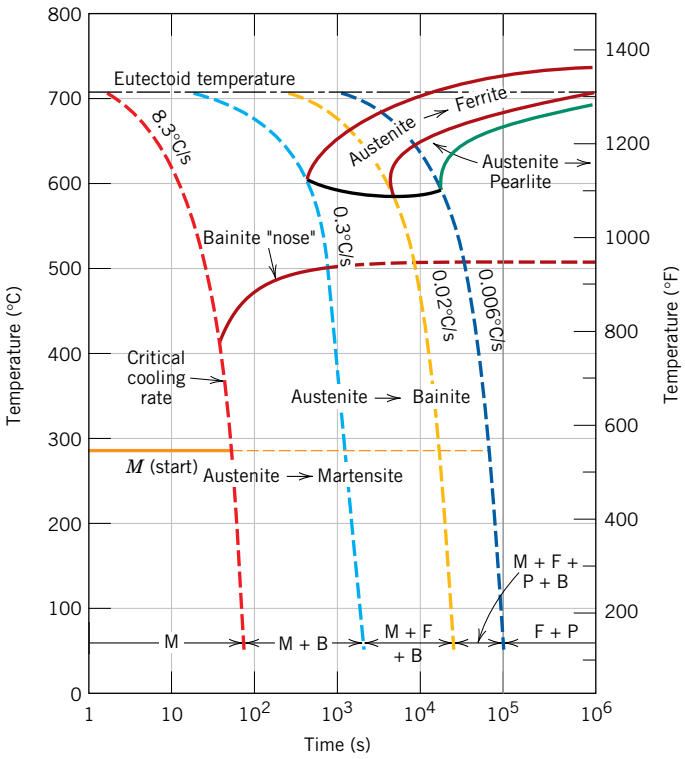

Figure 10.28 Continuous-cooling transformation diagram for an alloy steel (type 4340) and several superimposed cooling curves demonstrating dependence of the final microstructure of this alloy on the transformations that occur during cooling.
[Adapted from H. E. McGannon (Editor), *The Making, Shaping and Treating of Steel,* 9th edition, United States Steel Corporation, Pittsburgh, 1971, p. 1096.]

Concept Check 10.4 Briefly describe the simplest continuous cooling heat treatment procedure that would be used to convert a 4340 steel from (martensite + bainite) into (ferrite + pearlite).

[*The answer may be found at www.wiley.com/college/callister (Student Companion Site).*]

10.7 MECHANICAL BEHAVIOR OF IRON–CARBON ALLOYS

We now discuss the mechanical behavior of iron–carbon alloys having the microstructures discussed heretofore—namely, fine and coarse pearlite, spheroidite, bainite, and martensite. For all but martensite, two phases are present (ferrite and cementite), and so an opportunity is provided to explore several mechanical property–microstructure relationships that exist for these alloys.

Pearlite

Cementite is much harder but more brittle than ferrite. Thus, increasing the fraction of Fe_3C in a steel alloy while holding other microstructural elements constant will result in a harder and stronger material. This is demonstrated in Figure 10.29*a*, in which the tensile and yield strengths and the Brinell hardness number are plotted as a function of the weight percent carbon (or equivalently as the percentage of Fe_3C) for steels that are composed of fine pearlite. All three parameters increase with increasing carbon concentration. Inasmuch as cementite is more brittle, increasing its content results in a decrease in both ductility and toughness (or impact energy). These effects are shown in Figure 10.29*b* for the same fine pearlitic steels.

The layer thickness of each of the ferrite and cementite phases in the microstructure also influences the mechanical behavior of the material. Fine pearlite is harder and

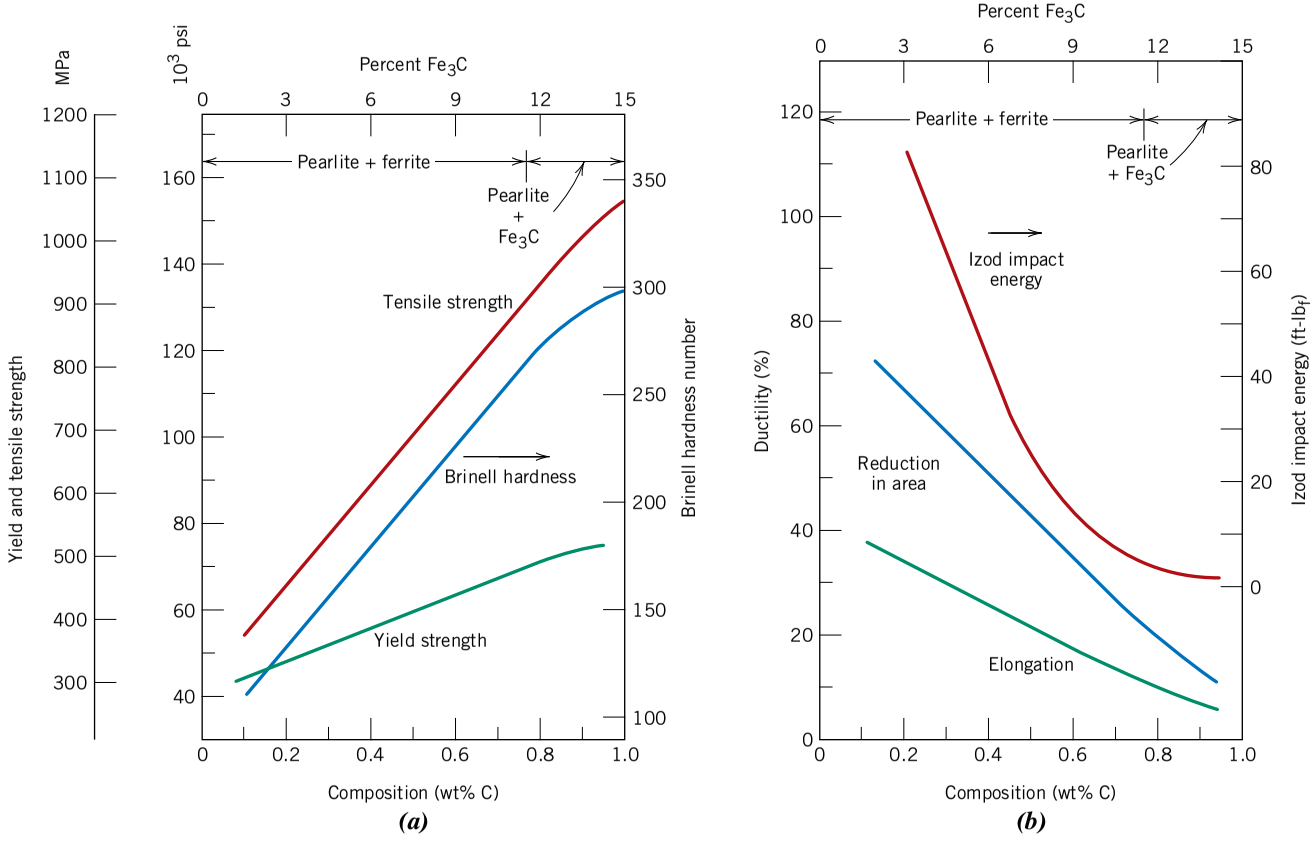

Figure 10.29 (*a*) Yield strength, tensile strength, and Brinell hardness versus carbon concentration for plain carbon steels having microstructures consisting of fine pearlite. (*b*) Ductility (%EL and %RA) and Izod impact energy versus carbon concentration for plain carbon steels having microstructures consisting of fine pearlite.
[Data taken from *Metals Handbook: Heat Treating,* Vol. 4, 9th edition, V. Masseria (Managing Editor), 1981. Reproduced by permission of ASM International, Materials Park, OH.]

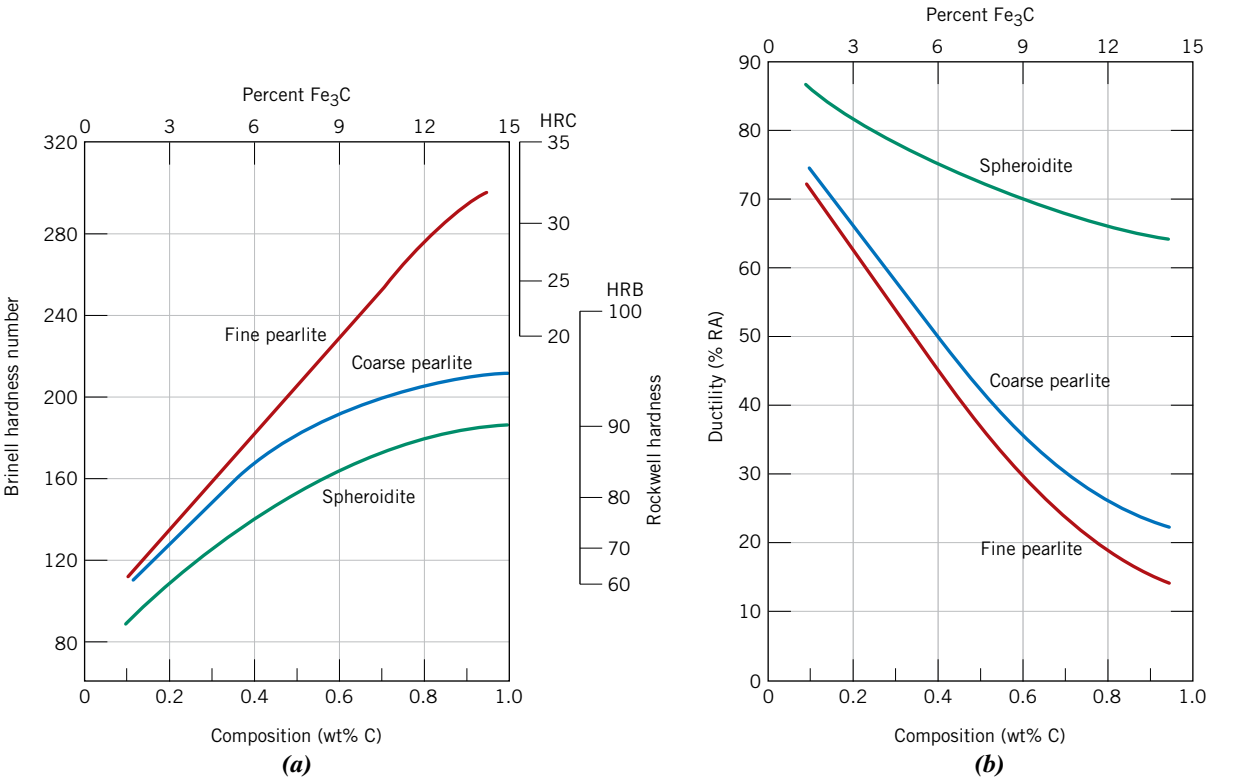

Figure 10.30 (*a*) Brinell and Rockwell hardness as a function of carbon concentration for plain carbon steels having fine and coarse pearlite as well as spheroidite microstructures. (*b*) Ductility (%RA) as a function of carbon concentration for plain carbon steels having fine and coarse pearlite as well as spheroidite microstructures. [Data taken from *Metals Handbook: Heat Treating,* Vol. 4, 9th edition, V. Masseria (Managing Editor), 1981. Reproduced by permission of ASM International, Materials Park, OH.]

stronger than coarse pearlite, as demonstrated by the upper two curves of Figure 10.30*a*, which plots hardness versus the carbon concentration.

The reasons for this behavior relate to phenomena that occur at the α–Fe_3C phase boundaries. First, there is a large degree of adherence between the two phases across a boundary. Therefore, the strong and rigid cementite phase severely restricts deformation of the softer ferrite phase in the regions adjacent to the boundary; thus the cementite may be said to reinforce the ferrite. The degree of this reinforcement is substantially higher in fine pearlite because of the greater phase boundary area per unit volume of material. In addition, phase boundaries serve as barriers to dislocation motion in much the same way as grain boundaries (Section 7.8). For fine pearlite there are more boundaries through which a dislocation must pass during plastic deformation. Thus, the greater reinforcement and restriction of dislocation motion in fine pearlite account for its greater hardness and strength.

Coarse pearlite is more ductile than fine pearlite, as illustrated in Figure 10.30*b*, which plots percentage reduction in area versus carbon concentration for both microstructure types. This behavior results from the greater restriction to plastic deformation of the fine pearlite.

Spheroidite

Other elements of the microstructure relate to the shape and distribution of the phases. In this respect, the cementite phase has distinctly different shapes and arrangements in the pearlite and spheroidite microstructures (Figures 10.15 and 10.19). Alloys containing pearlitic microstructures have greater strength and hardness than do those with spheroidite. This is demonstrated in Figure 10.30*a*, which compares the hardness as a function of the

weight percent carbon for spheroidite with both the pearlite structure types. This behavior is again explained in terms of reinforcement at, and impedance to, dislocation motion across the ferrite–cementite boundaries as discussed previously. There is less boundary area per unit volume in spheroidite, and consequently plastic deformation is not nearly as constrained, which gives rise to a relatively soft and weak material. In fact, of all steel alloys, those that are softest and weakest have a spheroidite microstructure.

As might be expected, spheroidized steels are extremely ductile, much more than either fine or coarse pearlite (Figure 10.30*b*). In addition, they are notably tough because any crack can encounter only a very small fraction of the brittle cementite particles as it propagates through the ductile ferrite matrix.

Bainite

Because bainitic steels have a finer structure (i.e., smaller α-ferrite and Fe_3C particles), they are generally stronger and harder than pearlitic steels; yet they exhibit a desirable combination of strength and ductility. Figures 10.31*a* and 10.31*b* show, respectively, the influence of transformation temperature on the strength/hardness and ductility for an iron–carbon alloy of eutectoid composition. Temperature ranges over which pearlite and bainite form (consistent with the isothermal transformation diagram for this alloy, Figure 10.18) are noted at the tops of Figures 10.31*a* and 10.31*b*.

Martensite

Of the various microstructures that may be produced for a given steel alloy, martensite is the hardest and strongest and, in addition, the most brittle; it has, in fact, negligible ductility. Its hardness is dependent on the carbon content, up to about 0.6 wt% as demonstrated in Figure 10.32, which plots the hardness of martensite and fine pearlite as a function of weight percent carbon. In contrast to pearlitic steels, the strength and hardness of martensite are not thought to be related to microstructure. Rather, these properties are attributed to the effectiveness of the interstitial carbon atoms in hindering dislocation motion (as a solid-solution effect, Section 7.9), and to the relatively few slip systems (along which dislocations move) for the BCT structure.

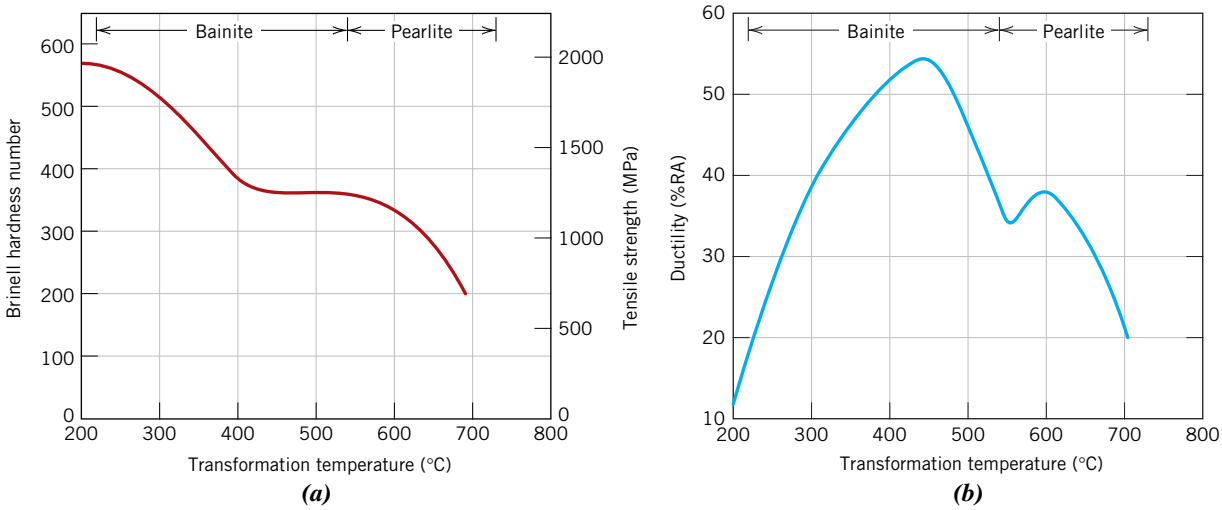

Figure 10.31 (*a*) Brinell hardness and tensile strength and (*b*) ductility (%RA) (at room temperature) as a function of isothermal transformation temperature for an iron–carbon alloy of eutectoid composition, taken over the temperature range at which bainitic and pearlitic microstructures form.
[Figure (*a*) Adapted from E. S. Davenport, "Isothermal Transformation in Steels," *Trans. ASM,* **27,** 1939, p. 847. Reprinted by permission of ASM International, Materials Park, OH.]

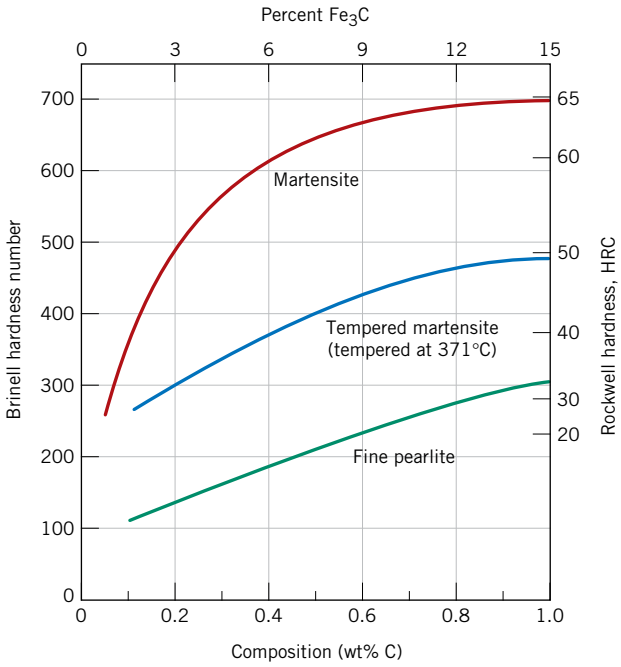

Figure 10.32 Hardness (at room temperature) as a function of carbon concentration for plain carbon martensitic, tempered martensitic [tempered at 371°C (700°F)], and pearlitic steels.
(Adapted from Edgar C. Bain, *Functions of the Alloying Elements in Steel,* 1939; and R. A. Grange, C. R. Hribal, and L. F. Porter, *Metall. Trans. A*, Vol. 8A. Reproduced by permission of ASM International, Materials Park, OH.)

Austenite is slightly denser than martensite, and therefore, during the phase transformation upon quenching, there is a net volume increase. Consequently, relatively large pieces that are rapidly quenched may crack as a result of internal stresses; this becomes a problem especially when the carbon content is greater than about 0.5 wt%.

Concept Check 10.5 Rank the following iron–carbon alloys and associated microstructures from the highest to the lowest tensile strength:

0.25 wt% C with spheroidite
0.25 wt% C with coarse pearlite
0.6 wt% C with fine pearlite
0.6 wt% C with coarse pearlite

Justify this ranking.

Concept Check 10.6 For a eutectoid steel, describe an isothermal heat treatment that would be required to produce a specimen having a hardness of 93 HRB.

[*The answers may be found at www.wiley.com/college/callister (Student Companion Site).*]

10.8 TEMPERED MARTENSITE

In the as-quenched state, martensite, in addition to being very hard, is so brittle that it cannot be used for most applications; also, any internal stresses that may have been introduced during quenching have a weakening effect. The ductility and toughness of martensite may be enhanced and these internal stresses relieved by a heat treatment known as *tempering.*

Tempering is accomplished by heating a martensitic steel to a temperature below the eutectoid for a specified time period. Normally, tempering is carried out at temperatures

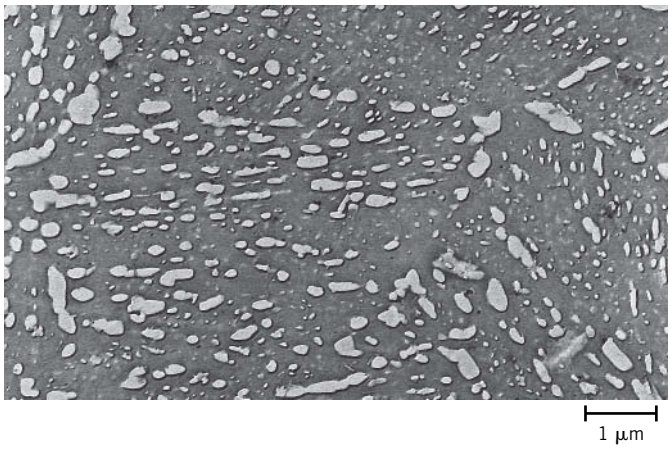

Figure 10.33 Electron micrograph of tempered martensite. Tempering was carried out at 594°C (1100°F). The small particles are the cementite phase; the matrix phase is α-ferrite. 9300×.
(Copyright 1971 by United States Steel Corporation.)

between 250°C and 650°C (480°F and 1200°F); internal stresses, however, may be relieved at temperatures as low as 200°C (390°F). This tempering heat treatment allows, by diffusional processes, the formation of **tempered martensite**, according to the reaction

tempered martensite

Martensite to tempered martensite transformation reaction

$$\text{martensite (BCT, single phase)} \rightarrow \text{tempered martensite } (\alpha + \text{Fe}_3\text{C phases}) \quad (10.20)$$

where the single-phase BCT martensite, which is supersaturated with carbon, transforms into the tempered martensite, composed of the stable ferrite and cementite phases, as indicated on the iron–iron carbide phase diagram.

The microstructure of tempered martensite consists of extremely small and uniformly dispersed cementite particles embedded within a continuous ferrite matrix. This is similar to the microstructure of spheroidite except that the cementite particles are much, much smaller. An electron micrograph showing the microstructure of tempered martensite at a very high magnification is presented in Figure 10.33.

Tempered martensite may be nearly as hard and strong as martensite but with substantially enhanced ductility and toughness. For example, the hardness-versus-weight percent carbon plot of Figure 10.32 includes a curve for tempered martensite. The hardness and strength may be explained by the large ferrite–cementite phase boundary area per unit volume that exists for the very fine and numerous cementite particles. Again, the hard cementite phase reinforces the ferrite matrix along the boundaries, and these boundaries also act as barriers to dislocation motion during plastic deformation. The continuous ferrite phase is also very ductile and relatively tough, which accounts for the improvement of these two properties for tempered martensite.

The size of the cementite particles influences the mechanical behavior of tempered martensite; increasing the particle size decreases the ferrite–cementite phase boundary area and, consequently, results in a softer and weaker material yet one that is tougher and more ductile. Furthermore, the tempering heat treatment determines the size of the cementite particles. Heat treatment variables are temperature and time, and most treatments are constant-temperature processes. Because carbon diffusion is involved in the martensite-tempered martensite transformation, increasing the temperature accelerates diffusion, the rate of cementite particle growth, and, subsequently, the rate of softening. The dependence of tensile and yield strength and ductility on tempering temperature for an alloy steel is shown in Figure 10.34. Before tempering, the material was quenched in oil to produce the martensitic structure; the tempering time at each temperature was 1 h. This type of tempering data is ordinarily provided by the steel manufacturer.

The time dependence of hardness at several different temperatures is presented in Figure 10.35 for a water-quenched steel of eutectoid composition; the time scale is

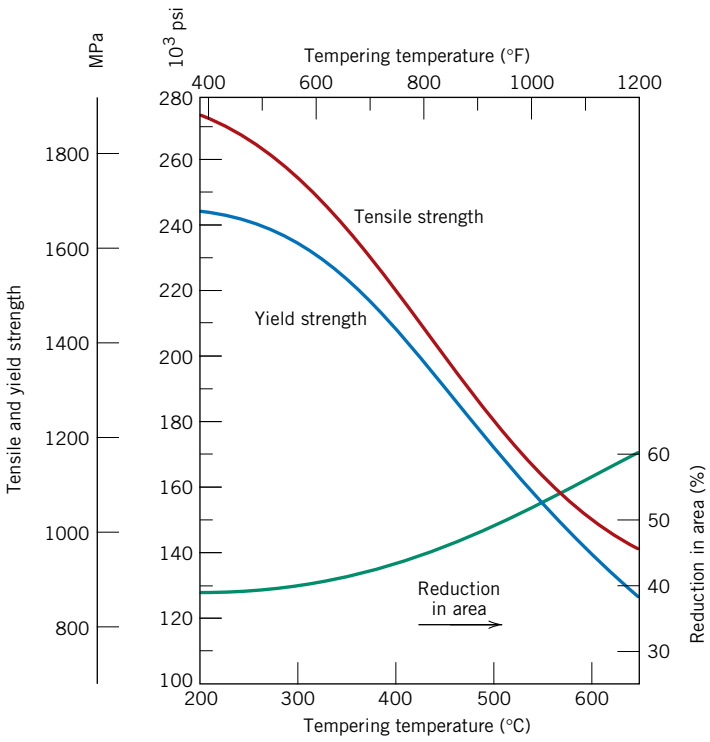

Figure 10.34 Tensile and yield strengths and ductility (%RA) (at room temperature) versus tempering temperature for an oil-quenched alloy steel (type 4340). (Adapted from Edgar C. Bain, *Functions of the Alloying Elements in Steel,* 1939. Reproduced by permission of ASM International, Materials Park, OH.)

logarithmic. With increasing time the hardness decreases, which corresponds to the growth and coalescence of the cementite particles. At temperatures approaching the eutectoid [700°C (1300°F)] and after several hours, the microstructure will become spheroiditic (Figure 10.19), with large cementite spheroids embedded within the continuous ferrite phase. Correspondingly, overtempered martensite is relatively soft and ductile.

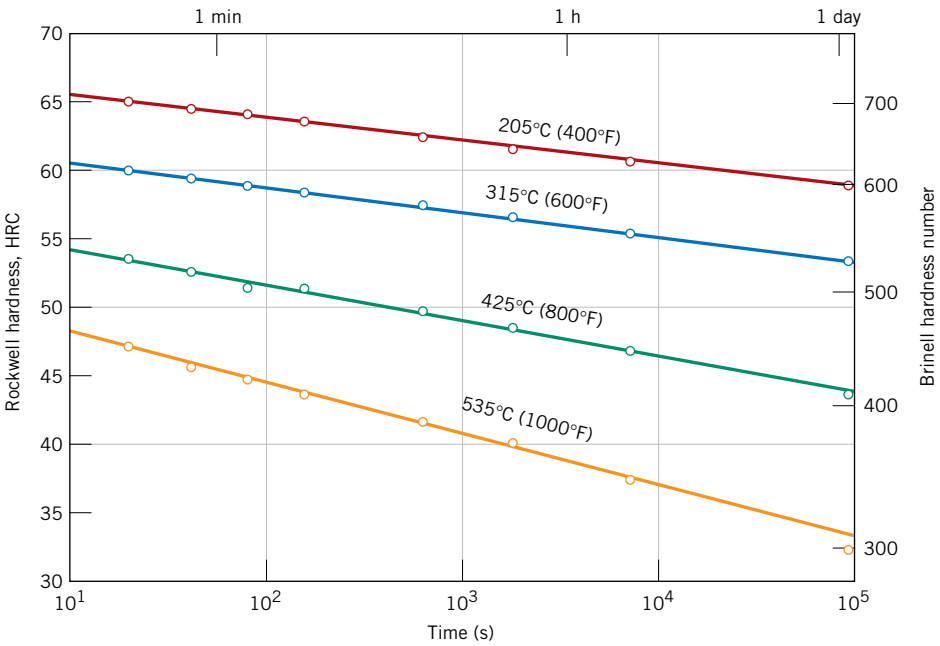

Figure 10.35 Hardness (at room temperature) versus tempering time for a water-quenched eutectoid plain carbon (1080) steel. (Adapted from Edgar C. Bain, *Functions of the Alloying Elements in Steel,* American Society for Metals, 1939, p. 233.)

Concept Check 10.7 A steel alloy is quenched from a temperature within the austenite phase region into water at room temperature so as to form martensite; the alloy is subsequently tempered at an elevated temperature, which is held constant.

(a) Make a schematic plot showing how room-temperature ductility varies with the logarithm of tempering time at the elevated temperature. (Be sure to label your axes.)

(b) Superimpose and label on this same plot the room-temperature behavior resulting from tempering at a higher temperature and briefly explain the difference in behavior at these two temperatures.

[*The answer may be found at www.wiley.com/college/callister (Student Companion Site).*]

The tempering of some steels may result in a reduction of toughness as measured by impact tests (Section 8.6); this is termed *temper embrittlement*. The phenomenon occurs when the steel is tempered at a temperature above about 575°C (1070°F) followed by slow cooling to room temperature, or when tempering is carried out at between approximately 375°C and 575°C (700°F and 1070°F). Steel alloys that are susceptible to temper embrittlement have been found to contain appreciable concentrations of the alloying elements manganese, nickel, or chromium and, in addition, one or more of antimony, phosphorus, arsenic, and tin as impurities in relatively low concentrations. The presence of these alloying elements and impurities shifts the ductile-to-brittle transition to significantly higher temperatures; the ambient temperature thus lies below this transition in the brittle regime. It has been observed that crack propagation of these embrittled materials is *intergranular* (Figure 8.7)—that is, the fracture path is along the grain boundaries of the precursor austenite phase. Furthermore, alloy and impurity elements have been found to preferentially segregate in these regions.

Temper embrittlement may be avoided by (1) compositional control and/or (2) tempering above 575°C or below 375°C, followed by quenching to room temperature. Furthermore, the toughness of steels that have been embrittled may be improved significantly by heating to about 600°C (1100°F) and then rapidly cooling to below 300°C (570°F).

10.9 REVIEW OF PHASE TRANSFORMATIONS AND MECHANICAL PROPERTIES FOR IRON–CARBON ALLOYS

In this chapter, we discussed several different microstructures that may be produced in iron–carbon alloys depending on heat treatment. Figure 10.36 summarizes the

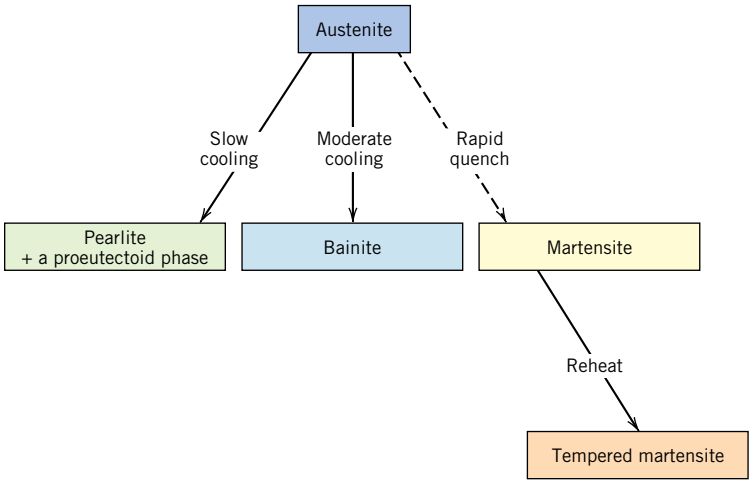

Figure 10.36 Possible transformations involving the decomposition of austenite. Solid arrows, transformations involving diffusion; dashed arrow, diffusionless transformation.

Table 10.2 Microstructures and Mechanical Properties for Iron–Carbon Alloys

Microconstituent	*Phases Present*	*Arrangement of Phases*	*Mechanical Properties (Relative)*
Spheroidite	α-Ferrite + Fe_3C	Relatively small Fe_3C spherelike particles in an α-ferrite matrix	Soft and ductile
Coarse pearlite	α-Ferrite + Fe_3C	Alternating layers of α-ferrite and Fe_3C that are relatively thick	Harder and stronger than spheroidite, but not as ductile as spheroidite
Fine pearlite	α-Ferrite + Fe_3C	Alternating layers of α-ferrite and Fe_3C that are relatively thin	Harder and stronger than coarse pearlite, but not as ductile as coarse pearlite
Bainite	α-Ferrite + Fe_3C	Very fine and elongated particles of Fe_3C in an α-ferrite matrix	Harder and stronger than fine pearlite; less hard than martensite; more ductile than martensite
Tempered martensite	α-Ferrite + Fe_3C	Very small Fe_3C spherelike particles in an α-ferrite matrix	Strong; not as hard as martensite, but much more ductile than martensite
Martensite	Body-centered, tetragonal, single phase	Needle-shaped grains	Very hard and very brittle

WileyPLUS

Tutorial Video: Iron–Carbon Alloy Microstructures
What are the Differences between the Various Iron–Carbon Alloy Microstructures?

transformation paths that produce these various microstructures. Here, it is assumed that pearlite, bainite, and martensite result from continuous-cooling treatments; furthermore, the formation of bainite is possible only for alloy steels (not plain carbon ones), as outlined earlier.

Microstructural characteristics and mechanical properties of the several microconstituents for iron–carbon alloys are summarized in Table 10.2.

EXAMPLE PROBLEM 10.4

Determination of Properties for a Eutectoid Fe–Fe_3C Alloy Subjected to an Isothermal Heat Treatment

Determine the tensile strength and ductility (%RA) of a eutectoid Fe–Fe_3C alloy that has been subjected to heat treatment (c) in Example Problem 10.3.

Solution

According to Figure 10.24, the final microstructure for heat treatment (c) consists of approximately 50% pearlite that formed during the 650°C isothermal heat treatment, whereas the remaining 50% austenite transformed to bainite at 400°C; thus, the final microstructure is 50% pearlite and 50% bainite. The tensile strength may be determined using Figure 10.31*a*. For pearlite, which was formed at an isothermal transformation temperature of 650°C, the tensile strength is approximately 950 MPa, whereas using this same plot, the bainite that formed at 400°C has an approximate tensile strength of 1300 MPa. Determination of these two tensile strength values is demonstrated in the following illustration.

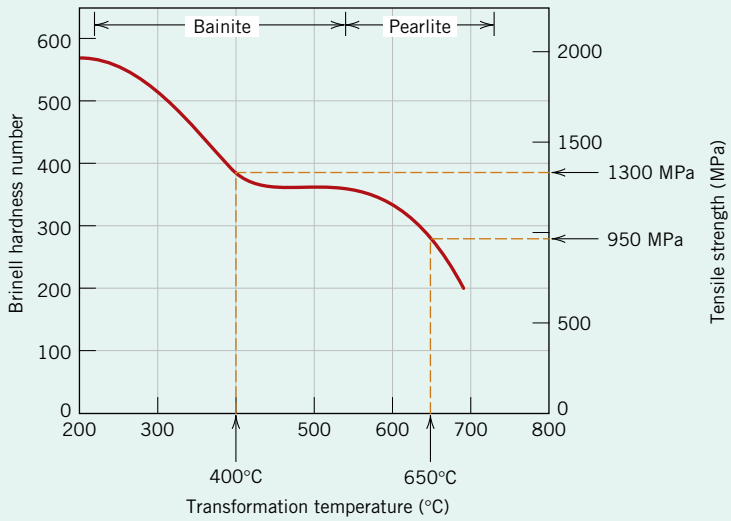

The tensile strength of this two-microconstituent alloy may be approximated using a "rule-of-mixtures" relationship—that is, the alloy tensile strength is equal to the fraction-weighted average of the two microconstituents, which may be expressed by the following equation:

$$\overline{TS} = W_p(TS)_p + W_b(TS)_b \tag{10.21}$$

Here,

$\overline{TS}$ = tensile strength of the alloy,

W_p and W_b = mass fractions of pearlite and bainite, respectively, and

$(TS)_p$ and $(TS)_b$ = tensile strengths of the respective microconstituents.

Thus, incorporating values for these four parameters into Equation 10.21 leads to the following alloy tensile strength:

$$\begin{aligned}\overline{TS} &= (0.50)(950\ \text{MPa}) + (0.50)(1300\ \text{MPa}) \\ &= 1125\ \text{MPa}\end{aligned}$$

This same technique is used for the computation of ductility. In this case, approximate ductility values for the two microconstituents, taken at 650°C (for pearlite) and 400°C (for bainite), are, respectively, 32%RA and 52%RA, as taken from the following adaptation of Figure 10.31*b*:

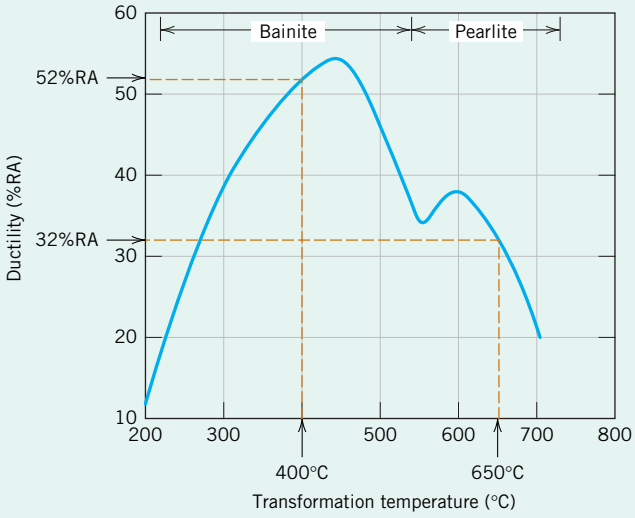

Adaptation of the rule-of-mixtures expression (Equation 10.21) for this case is as follows:

$$\%\overline{RA} = W_p(\%RA)_p + W_b(\%RA)_b$$

When values for the *W*s and %RAs are inserted into this expression, the approximate ductility is calculated as

$$\begin{aligned}\%\overline{RA} &= (0.50)(32\%RA) + (0.50)(52\%RA)\\ &= 42\%RA\end{aligned}$$

In summary, for the eutectoid alloy subjected to the specified isothermal heat treatment, tensile strength and ductility values are approximately 1125 MPa and 42%RA, respectively.

MATERIALS OF IMPORTANCE

Shape-Memory Alloys

A relatively new group of metals that exhibit an interesting (and practical) phenomenon are the *shape-memory alloys* (or *SMA*s). One of these materials, after being deformed, has the ability to return to its predeformed size and shape upon being subjected to an appropriate heat treatment—that is, the material "remembers" its previous size/shape. Deformation normally is carried out at a relatively low temperature, whereas shape memory occurs upon heating.[5] Materials that have been found to be capable of recovering significant amounts of deformation (i.e., strain) are nickel–titanium alloys (Nitinol,[6] is their trade name) and some copper-base alloys (Cu–Zn–Al and Cu–Al–Ni alloys).

A shape-memory alloy is polymorphic (Section 3.6)—that is, it may have two crystal structures (or phases), and the shape-memory effect involves phase transformations between them. One phase (termed an *austenite phase*) has a body-centered cubic structure that exists at elevated temperatures; its structure is represented schematically by the inset shown at stage 1 of Figure 10.37. Upon cooling, the austenite transforms spontaneously into a martensite phase, which is similar to the martensitic transformation for the iron–carbon system (Section 10.5)—that is, it is diffusionless, involves an orderly shift of large groups of atoms, and occurs very rapidly, and the degree of transformation is dependent on temperature; temperatures at which the transformation begins and ends are indicated by M_s and M_f labels, respectively, on the left vertical axis of Figure 10.37. In addition, this martensite is heavily twinned,[7] as represented schematically by the stage 2

Time-lapse photograph that demonstrates the shape-memory effect. A wire of a shape-memory alloy (Nitinol) has been bent and treated such that its memory shape spells the word *Nitinol*. The wire is then deformed and, upon heating (by passage of an electric current), springs back to its predeformed shape; this shape recovery process is recorded on the photograph. [Photograph courtesy the Naval Surface Warfare Center (previously the Naval Ordnance Laboratory)].

[5]Alloys that demonstrate this phenomenon only upon heating are said to have a *one-way* shape memory. Some of these materials experience size/shape changes on both heating and cooling; these are termed *two-way* shape memory alloys. In this discussion, we discuss the mechanism for only the one-way shape memory alloys.

[6]*Nitinol* is an acronym for *ni*ckel-*ti*tanium *N*aval *O*rdnance *L*aboratory, where this alloy was discovered.

[7]The phenomenon of twinning is described in Section 7.7.

inset of Figure 10.37. Under the influence of an applied stress, deformation of martensite (i.e., the passage from stage 2 to stage 3 in Figure 10.37) occurs by the migration of twin boundaries—some twinned regions grow while others shrink; this deformed martensitic structure is represented by the stage 3 inset. Furthermore, when the stress is removed, the deformed shape is retained at this temperature. Finally, upon subsequent heating to the initial temperature, the material reverts back to (i.e., "remembers") its original size and shape (stage 4). This stage 3–stage 4 process is accompanied by a phase transformation from the deformed martensite into the original high-temperature austenite phase. For these shape-memory alloys, the martensite-to-austenite transformation occurs over a temperature range, between the temperatures denoted by A_s (austenite start) and A_f (austenite finish) labels on the right vertical axis of Figure 10.37. This deformation–transformation cycle may be repeated for the shape-memory material.

The original shape (the one that is to be remembered) is created by heating to well above the A_f temperature (such that the transformation to austenite is complete) and then restraining the material to the desired memory shape for a sufficient time period. For example, for Nitinol alloys, a 1-h treatment at 500°C is necessary.

Although the deformation experienced by shape-memory alloys is semipermanent, it is not truly "plas-

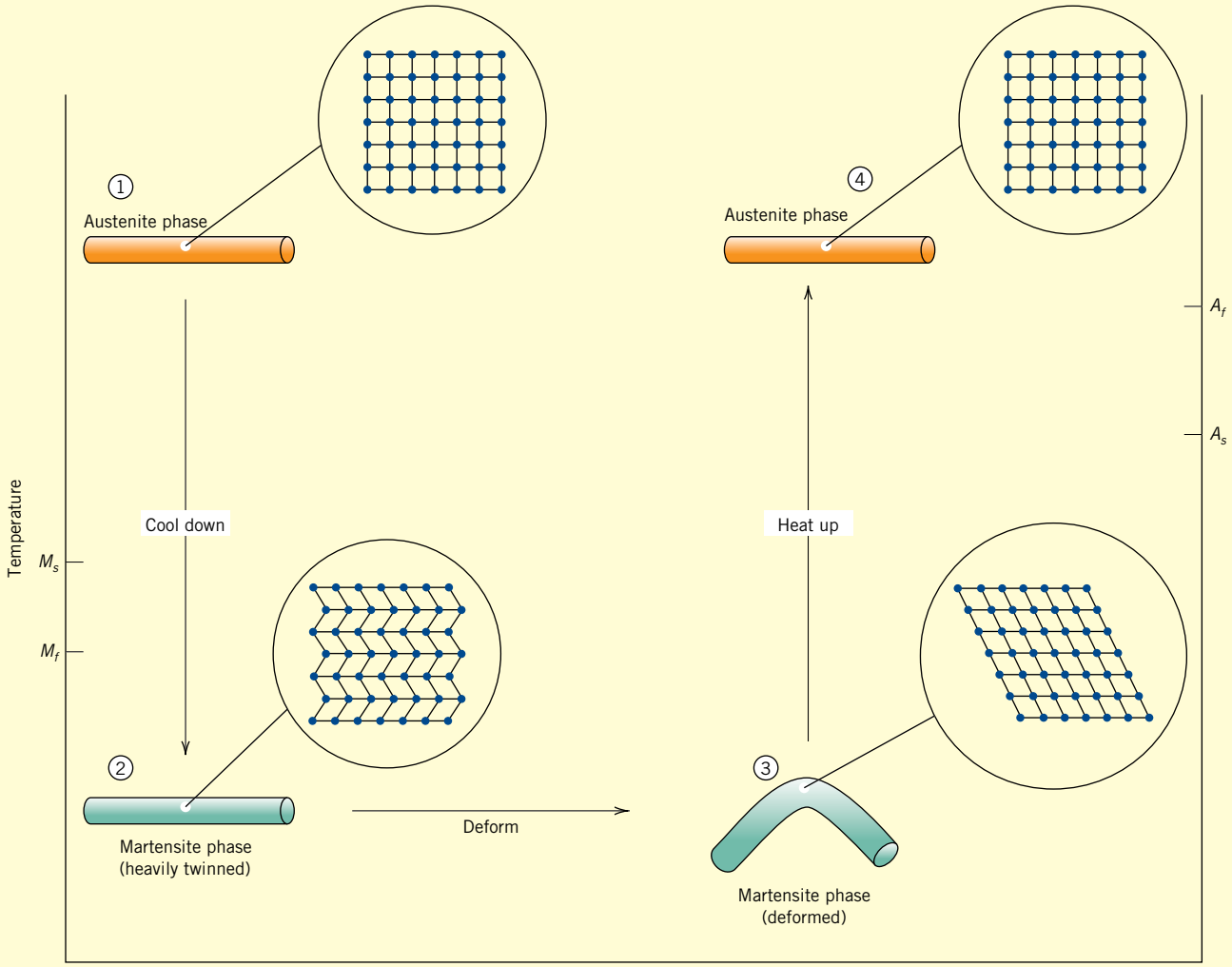

Figure 10.37 Diagram illustrating the shape-memory effect. The insets are schematic representations of the crystal structure at the four stages. M_s and M_f denote temperatures at which the martensitic transformation begins and ends, respectively. Likewise for the austenite transformation, A_s and A_f represent the respective beginning and end transformation temperatures.

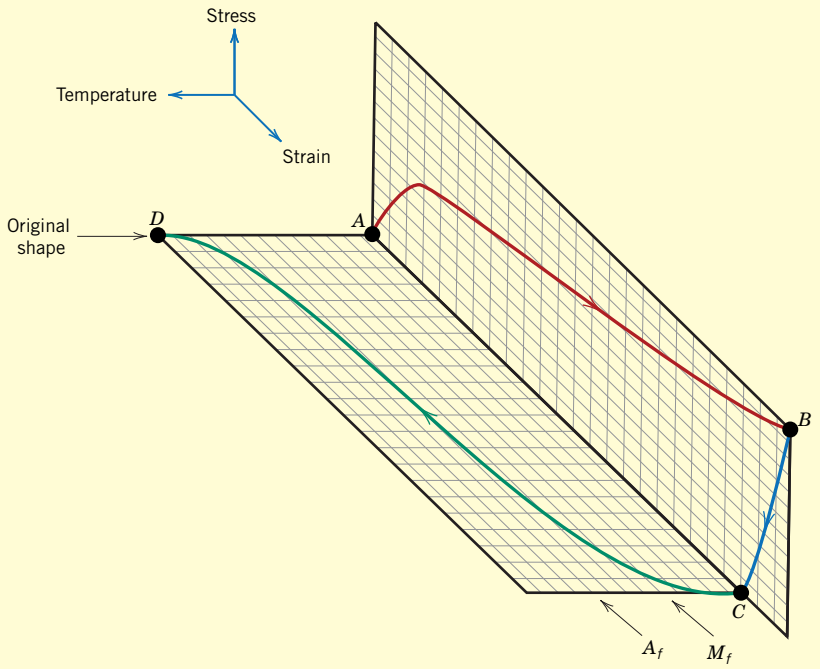

Figure 10.38 Typical stress-strain-temperature behavior of a shape-memory alloy, demonstrating its thermoelastic behavior. Specimen deformation, corresponding to the curve from *A* to *B*, is carried out at a temperature below that at which the martensitic transformation is complete (i.e., M_f of Figure 10.37). Release of the applied stress (also at M_f) is represented by the curve *BC*. Subsequent heating to above the completed austenite-transformation temperature (A_f, Figure 10.37) causes the deformed piece to resume its original shape (along the curve from point *C* to point *D*).
[From Helsen, J. A., and H. J. Breme (Editors), *Metals as Biomaterials,* John Wiley & Sons, Chichester, UK, 1998. Reprinted with permission of John Wiley & Sons Inc.]

tic" deformation, as discussed in Section 6.6, nor is it strictly "elastic" (Section 6.3). Rather, it is termed *thermoelastic,* because deformation is nonpermanent when the deformed material is subsequently heat-treated. The stress-strain-temperature behavior of a thermoelastic material is presented in Figure 10.38. Maximum recoverable deformation strains for these materials are on the order of 8%.

For this Nitinol family of alloys, transformation temperatures can be made to vary over a wide temperature range (between about –200°C and 110°C) by altering the Ni–Ti ratio and also by adding other elements.

One important SMA application is in weldless, shrink-to-fit pipe couplers used for hydraulic lines on aircraft, for joints on undersea pipelines, and for plumbing on ships and submarines. Each coupler (in the form of a cylindrical sleeve) is fabricated so as to have an inside diameter slightly smaller than the outside diameter of the pipes to be joined. It is then stretched (circumferentially) at some temperature well below the ambient temperature. Next the coupler is fitted over the pipe junction and then heated to room temperature; heating causes the coupler to shrink back to its original diameter, thus creating a tight seal between the two pipe sections.

There is a host of other applications for alloys displaying this effect—for example, eyeglass frames, tooth-straightening braces, collapsible antennas, greenhouse window openers, antiscald control valves on showers, women's foundation-garments, fire sprinkler valves, and biomedical applications (such as blood-clot filters, self-extending coronary stents, and bone anchors). Shape-memory alloys also fall into the classification of "smart materials" (Section 1.5) because they sense and respond to environmental (i.e., temperature) changes.

SUMMARY

The Kinetics of Phase Transformations

- Nucleation and growth are the two steps involved in the production of a new phase.
- Two types of nucleation are possible: homogeneous and heterogeneous.
  - For homogeneous nucleation, nuclei of the new phase form uniformly throughout the parent phase.
  - For heterogeneous nucleation, nuclei form preferentially at the surfaces of structural inhomogeneities (e.g., container surfaces, insoluble impurities).
- For the homogeneous nucleation of a spherical solid particle in a liquid solution, expressions for the critical radius (r^*) and activation free energy (ΔG^*) are represented by Equations 10.3 and 10.4, respectively. These two parameters are indicated in the plot of Figure 10.2*b*.
- The activation free energy for heterogeneous nucleation (ΔG^*_{het}) is lower than that for homogeneous nucleation (ΔG^*_{hom}), as demonstrated on the schematic free energy–versus–nucleus radius curves of Figure 10.6.
- Heterogeneous nucleation occurs more easily than homogeneous nucleation, which is reflected in a smaller degree of supercooling (ΔT) for the former—that is, $\Delta T_{het} < \Delta T_{hom}$, Figure 10.7.
- The growth stage of phase particle formation begins once a nucleus has exceeded the critical radius (r^*).
- For typical solid transformations, a plot of fraction transformation versus logarithm of time yields an S-shaped curve, as depicted schematically in Figure 10.10.
- The time dependence of degree of transformation is represented by the Avrami equation, Equation 10.17.
- Transformation rate is taken as the reciprocal of time required for a transformation to proceed halfway to its completion, Equation 10.18.
- For transformations that are induced by temperature alterations, when the rate of temperature change is such that equilibrium conditions are not maintained, transformation temperature is raised (for heating) and lowered (for cooling). These phenomena are termed superheating and supercooling, respectively.

Isothermal Transformation Diagrams

Continuous-Cooling Transformation Diagrams

- Phase diagrams provide no information as to the time dependence of transformation progress. However, the element of time is incorporated into isothermal transformation diagrams. These diagrams do the following:
  - Plot temperature versus the logarithm of time, with curves for beginning, as well as 50% and 100% transformation completion.
  - Are generated from a series of plots of percentage transformation versus the logarithm of time taken over a range of temperatures (Figure 10.13).
  - Are valid only for constant-temperature heat treatments.
  - Permit determination of times at which a phase transformation begins and ends.
- Isothermal transformation diagrams may be modified for continuous-cooling heat treatments; isothermal transformation beginning and ending curves are shifted to longer times and lower temperatures (Figure 10.25). Intersections with these curves of continuous-cooling curves represent times at which the transformation starts and ceases.

- Isothermal and continuous-cooling transformation diagrams make possible the prediction of microstructural products for specified heat treatments. This feature was demonstrated for alloys of iron and carbon.
- Microstructural products for iron–carbon alloys are as follows:
  - Coarse and fine pearlite—the alternating α-ferrite and cementite layers are thinner for fine than for coarse pearlite. Coarse pearlite forms at higher temperatures (isothermally) and for slower cooling rates (continuous cooling).
  - Bainite—this has a very fine structure that is composed of a ferrite matrix and elongated cementite particles. It forms at lower temperatures/higher cooling rates than fine pearlite.
  - Spheroidite—this is composed of spherelike cementite particles that are embedded in a ferrite matrix. Heating fine/coarse pearlite or bainite at about 700°C for several hours produces spheroidite.
  - Martensite—this has platelike or needle-like grains of an iron–carbon solid solution that has a body-centered tetragonal crystal structure. Martensite is produced by rapidly quenching austenite to a sufficiently low temperature so as to prevent carbon diffusion and the formation of pearlite and/or bainite.
  - Tempered martensite—this consists of very small cementite particles within a ferrite matrix. Heating martensite at temperatures within the range of about 250°C to 650°C results in its transformation to tempered martensite.
- The addition of some alloying elements (other than carbon) shifts pearlite and bainite noses on a continuous-cooling transformation diagram to longer times, making the transformation to martensite more favorable (and an alloy more heat-treatable).

Mechanical Behavior of Iron–Carbon Alloys

- Martensitic steels are the hardest and strongest, yet most brittle.
- Tempered martensite is very strong but relatively ductile.
- Bainite has desirable strength-ductility combination but is not as strong as tempered martensite.
- Fine pearlite is harder, stronger, and more brittle than coarse pearlite.
- Spheroidite is the softest and most ductile of the microstructures discussed.
- Embrittlement of some steel alloys results when specific alloying and impurity elements are present and upon tempering within a definite temperature range.

Shape-Memory Alloys

- These alloys may be deformed and then return to their predeformed sizes/shapes upon heating.
- Deformation occurs by the migration of twin boundaries. A martensite-to-austenite phase transformation accompanies the reversion back to the original size/shape.

Equation Summary

Equation Number	*Equation*	*Solving For*	*Page Number*
10.3	$r^* = -\dfrac{2\gamma}{\Delta G_v}$	Critical radius for stable solid particle (homogeneous nucleation)	360
10.4	$\Delta G^* = \dfrac{16\pi\gamma^3}{3(\Delta G_v)^2}$	Activation free energy for formation of stable solid particle (homogeneous nucleation)	360

(*continued*)

Equation Number	Equation	Solving For	Page Number
10.6	$r^* = \left(-\frac{2\gamma T_m}{\Delta H_f}\right)\left(\frac{1}{T_m - T}\right)$	Critical radius—in terms of latent heat of fusion and melting temperature	360
10.7	$\Delta G^* = \left(\frac{16\pi\gamma^3 T_m^2}{3\Delta H_f^2}\right)\frac{1}{(T_m - T)^2}$	Activation free energy—in terms of latent heat of fusion and melting temperature	360
10.12	$\gamma_{IL} = \gamma_{SI} + \gamma_{SL}\cos\theta$	Relationship among interfacial energies for heterogeneous nucleation	364
10.13	$r^* = -\frac{2\gamma_{SL}}{\Delta G_v}$	Critical radius for stable solid particle (heterogeneous nucleation)	364
10.14	$\Delta G^* = \left(\frac{16\pi\gamma_{SL}^3}{3\Delta G_v^2}\right)S(\theta)$	Activation free energy for formation of stable solid particle (heterogeneous nucleation)	364
10.17	$y = 1 - \exp(-kt^n)$	Fraction of transformation (Avrami equation)	368
10.18	$\text{rate} = \frac{1}{t_{0.5}}$	Transformation rate	368

List of Symbols

Symbol	Meaning
ΔG_v	Volume free energy
ΔH_f	Latent heat of fusion
k, n	Time-independent constants
$S(\theta)$	Nucleus shape function
T	Temperature (K)
T_m	Equilibrium solidification temperature (K)
$t_{0.5}$	Time required for a transformation to proceed to 50% completion
γ	Surface free energy
γ_{IL}	Liquid-surface interfacial energy (Figure 10.5)
γ_{SL}	Solid-liquid interfacial energy
γ_{SI}	Solid-surface interfacial energy
θ	Wetting angle (angle between γ_{SI} and γ_{SL} vectors) (Figure 10.5)

Processing/Structure/Properties/Performance Summary

For iron–carbon alloys, in addition to discussions of the heat treatments that produce the several microconstituents (fine/coarse pearlite, bainite, martensite, etc.) and their mechanical properties, correlations were made between mechanical properties and structural elements of these microconstituents. These correlations are indicated in the following concept map:

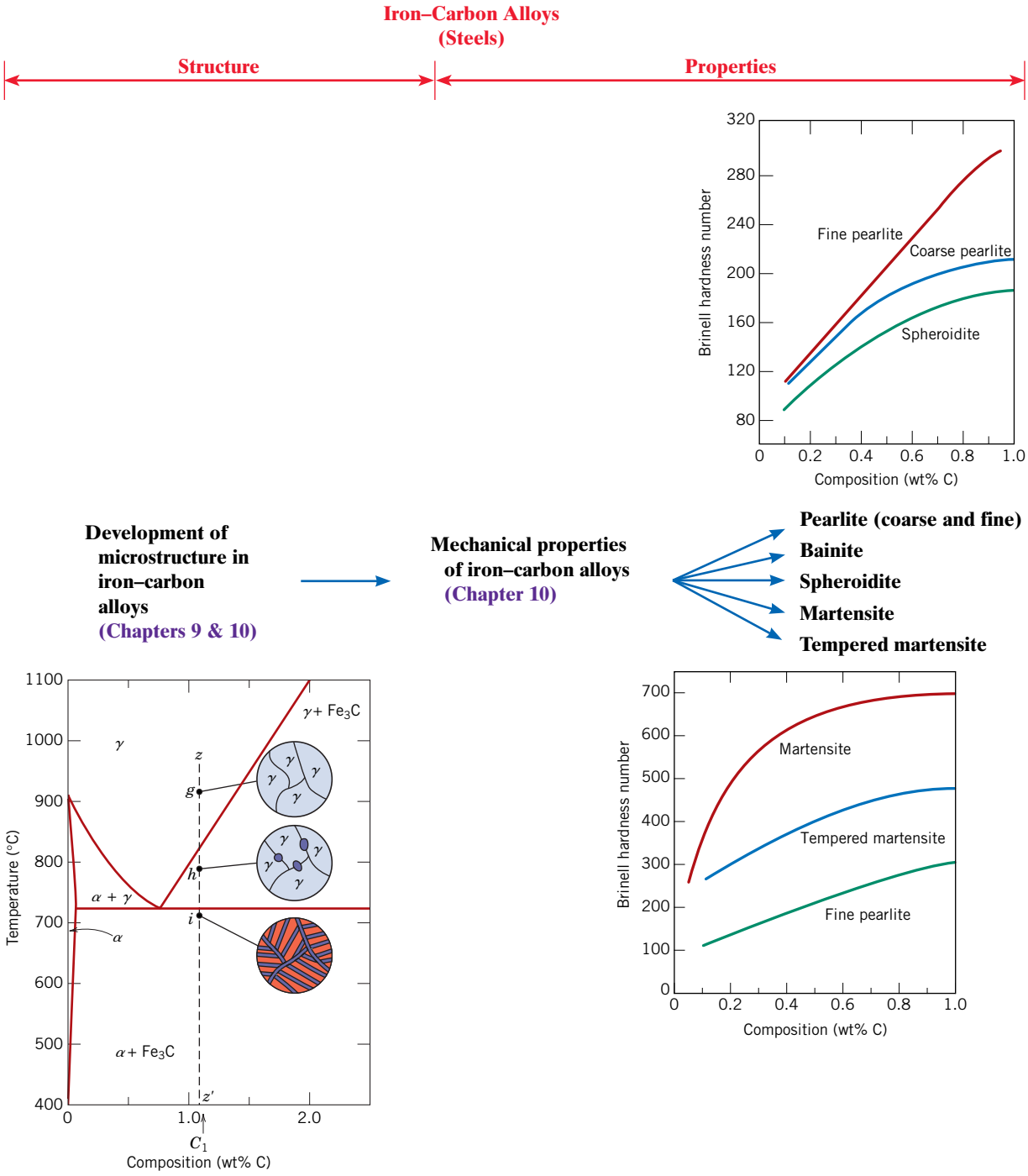

Furthermore, reference to the heat treating of steels (as discussed in Chapter 11) normally means tempering of martensite to form tempered martensite. An understanding of the conditions under which martensite forms is facilitated by utilizing continuous-cooling and isothermal transformation diagrams (Sections 10.5 and 10.6). In addition, these diagrams are just extensions of the iron–iron carbide phase diagram (Section 9.18). The following concept map notes these relationships:

Iron–Carbon Alloys
(Steels)
(Processing)

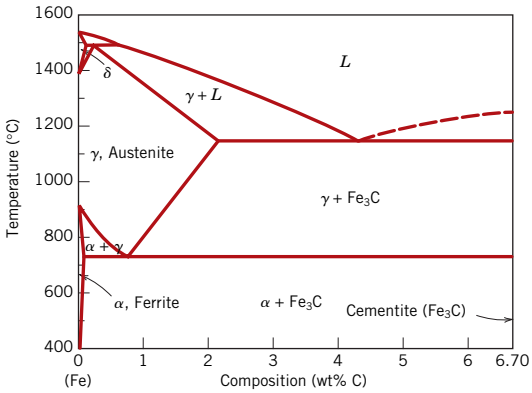

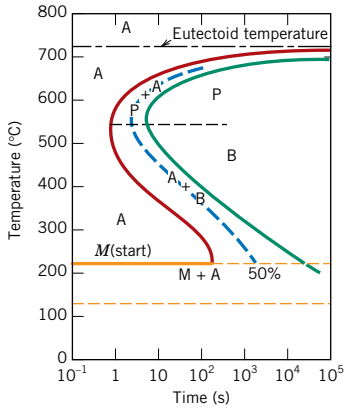

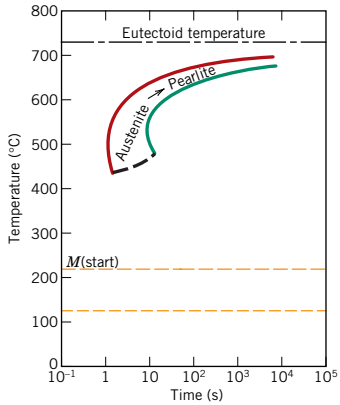

Iron–iron carbide phase diagram (Chapter 9) → **Isothermal transformation diagrams** (Chapter 10) → **Continuous-cooling transformation diagrams** (Chapter 10)

Martensite (formation of) (Chapter 10) → **Tempering (tempered martensite)** (Chapter 10) → **Heat treatment of steels** (Chapter 11)

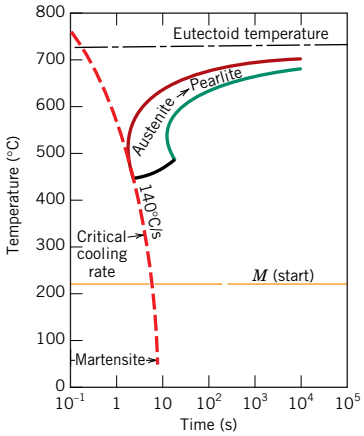

martensite (BCT, single phase) → tempered martensite (α + Fe_3C phases)

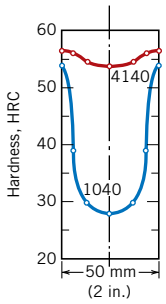

Important Terms and Concepts

alloy steel
athermal transformation
bainite
coarse pearlite
continuous-cooling transformation diagram
fine pearlite
free energy
growth (phase particle)
isothermal transformation diagram
kinetics
martensite
nucleation
phase transformation
plain carbon steel
spheroidite
supercooling
superheating
tempered martensite
thermally activated transformation
transformation rate

REFERENCES

Brooks, C. R., *Principles of the Heat Treatment of Plain Carbon and Low Alloy Steels,* ASM International, Materials Park, OH, 1996.

Krauss, G., *Steels: Processing, Structure, and Performance,* ASM International, Materials Park, OH, 2005.

Porter, D. A., K. E. Easterling, and M. Sherif, *Phase Transformations in Metals and Alloys,* 3rd edition, CRC Press, Boca Raton, FL, 2009.

Shewmon, P. G., *Transformations in Metals*, Indo American Books, Abbotsford, B.C., Canada, 2007.

Tarin, P., and J. Pérez, *SteCal®* 3.0 (Book and CD), ASM International, Materials Park, OH, 2004.

Vander Voort, G. (Editor), *Atlas of Time–Temperature Diagrams for Irons and Steels,* ASM International, Materials Park, OH, 1991.

Vander Voort, G. (Editor), *Atlas of Time–Temperature Diagrams for Nonferrous Alloys,* ASM International, Materials Park, OH, 1991.

QUESTIONS AND PROBLEMS

⊕ *Problem available (at instructor's discretion) in* WileyPLUS

The Kinetics of Phase Transformations

10.1 Name the two stages involved in the formation ⊕ of particles of a new phase. Briefly describe each.

10.2 (a) Rewrite the expression for the total free energy change for nucleation (Equation 10.1) for the case of a cubic nucleus of edge length a (instead of a sphere of radius r). Now differentiate this expression with respect to a (per Equation 10.2) and solve for both the critical cube edge length, a^*, and ΔG^*.

(b) Is ΔG^* greater for a cube or a sphere? Why?

10.3 If ice homogeneously nucleates at −40°C, cal- ⊕ culate the critical radius given values of -3.1×10^8 J/m^3 and 25×10^{-3} J/m^2, respectively, for the latent heat of fusion and the surface free energy.

10.4 (a) For the solidification of nickel, calculate the ⊕ critical radius r^* and the activation free energy ΔG^* if nucleation is homogeneous. Values for the latent heat of fusion and surface free energy are -2.53×10^9 J/m^3 and 0.255 J/m^2, respectively. Use the supercooling value found in Table 10.1.

(b) Now, calculate the number of atoms found in a nucleus of critical size. Assume a lattice parameter of 0.360 nm for solid nickel at its melting temperature.

10.5 (a) Assume for the solidification of nickel (Problem 10.4) that nucleation is homogeneous and that the number of stable nuclei is 10^6 nuclei per cubic meter. Calculate the critical radius and the number of stable nuclei that exist at the following degrees of supercooling: 200 and 300 K.

(b) What is significant about the magnitudes of these critical radii and the numbers of stable nuclei?

10.6 For some transformation having kinetics that ⊕ obey the Avrami equation (Equation 10.17), the parameter n is known to have a value of 1.5. If the reaction is 25% complete after 125 s, how long (total time) will it take the transformation to go to 90% completion?

10.7 Compute the rate of some reaction that obeys ⊕ Avrami kinetics, assuming that the constants n and k have values of 2.0 and 5×10^{-4}, respectively, for time expressed in seconds.

10.8 It is known that the kinetics of recrystallization ⊕ for some alloy obeys the Avrami equation, and that the value of n in the exponential is 5.0. If, at some temperature, the fraction recrystallized is 0.30 after 100 min, determine the rate of recrystallization at this temperature.

10.9 It is known that the kinetics of some transformation obeys the Avrami equation and that the value of k is 2.6×10^{-6} (for time in minutes). If the fraction recrystallized is 0.65 after 120 min, determine the rate of this transformation.

10.10 The kinetics of the austenite-to-pearlite trans- ⊕ formation obeys the Avrami relationship. Using the fraction transformed–time data given here, determine the total time required for 95% of the austenite to transform to pearlite.

Fraction Transformed	*Time (s)*
0.2	280
0.6	425

10.11 The fraction recrystallized–time data for the ⊕ recrystallization at 350°C of a previously deformed aluminum are tabulated here. Assuming that the kinetics of this process obey the Avrami relationship, determine the fraction recrystallized after a total time of 116.8 min.

Fraction Recrystallized	*Time (min)*
0.30	95.2
0.80	126.6

10.12 **(a)** From the curves shown in Figure 10.11 and using Equation 10.18, determine the rate of recrystallization for pure copper at the several temperatures.

(b) Make a plot of ln(rate) versus the reciprocal of temperature (in K^{-1}), and determine the activation energy for this recrystallization process. (See Section 5.5.)

(c) By extrapolation, estimate the length of time required for 50% recrystallization at room temperature, 20°C (293 K).

10.13 Determine values for the constants n and k (Equation 10.17) for the recrystallization of copper (Figure 10.11) at 119°C.

Metastable versus Equilibrium States

10.14 In terms of heat treatment and the development of microstructure, what are two major limitations of the iron–iron carbide phase diagram?

10.15 **(a)** Briefly describe the phenomena of superheating and supercooling.

(b) Why do these phenomena occur?

Isothermal Transformation Diagrams

10.16 Suppose that a steel of eutectoid composition is cooled to 675°C (1250°F) from 760°C (1400°F) in less than 0.5 s and held at this temperature.

(a) How long will it take for the austenite-to-pearlite reaction to go to 50% completion? To 100% completion?

(b) Estimate the hardness of the alloy that has completely transformed to pearlite.

10.17 Briefly cite the differences among pearlite, bainite, and spheroidite relative to microstructure and mechanical properties.

10.18 What is the driving force for the formation of spheroidite?

10.19 Using the isothermal transformation diagram for an iron–carbon alloy of eutectoid composition (Figure 10.22), specify the nature of the final microstructure (in terms of microconstituents present and approximate percentages of each) of a small specimen that has been subjected to the following time–temperature treatments. In each case assume that the specimen begins at 760°C (1400°F) and that it has been held at this temperature long enough to have achieved a complete and homogeneous austenitic structure.

(a) Cool rapidly to 350°C (660°F), hold for 10^3 s, then quench to room temperature.

(b) Rapidly cool to 625°C (1160°F), hold for 10 s, then quench to room temperature.

(c) Rapidly cool to 600°C (1110°F), hold for 4 s, rapidly cool to 450°C (840°F), hold for 10 s, then quench to room temperature.

(d) Reheat the specimen in part (c) to 700°C (1290°F) for 20 h.

(e) Rapidly cool to 300°C (570°F), hold for 20 s, then quench to room temperature in water. Reheat to 425°C (800°F) for 10^3 s and slowly cool to room temperature.

(f) Cool rapidly to 665°C (1230°F), hold for 10^3 s, then quench to room temperature.

(g) Rapidly cool to 575°C (1065°F), hold for 20 s, rapidly cool to 350°C (660°F), hold for 100 s, then quench to room temperature.

(h) Rapidly cool to 350°C (660°F), hold for 150 s, then quench to room temperature.

10.20 Make a copy of the isothermal transformation diagram for an iron–carbon alloy of eutectoid composition (Figure 10.22) and then sketch and label time–temperature paths on this diagram to produce the following microstructures:

(a) 100% coarse pearlite

(b) 50% martensite and 50% austenite

(c) 50% coarse pearlite, 25% bainite, and 25% martensite

10.21 Using the isothermal transformation diagram for a 1.13 wt% C steel alloy (Figure 10.39), determine the final microstructure (in terms of just the microconstituents present) of a small specimen that has been subjected to the following time–temperature treatments. In each case assume that the specimen begins at 920°C (1690°F) and that it has been held at this temperature long enough to have achieved a complete and homogeneous austenitic structure.

(a) Rapidly cool to 250°C (480°F), hold for 10^3 s, then quench to room temperature.

(b) Rapidly cool to 775°C (1430°F), hold for 500 s, then quench to room temperature.

(c) Rapidly cool to 400°C (750°F), hold for 500 s, then quench to room temperature.

(d) Rapidly cool to 700°C (1290°F), hold at this temperature for 10^5 s, then quench to room temperature.

(e) Rapidly cool to 650°C (1200°F), hold at this temperature for 3 s, rapidly cool to 400°C (750°F), hold for 25 s, then quench to room temperature.

(f) Rapidly cool to 350°C (660°F), hold for 300 s, then quench to room temperature.

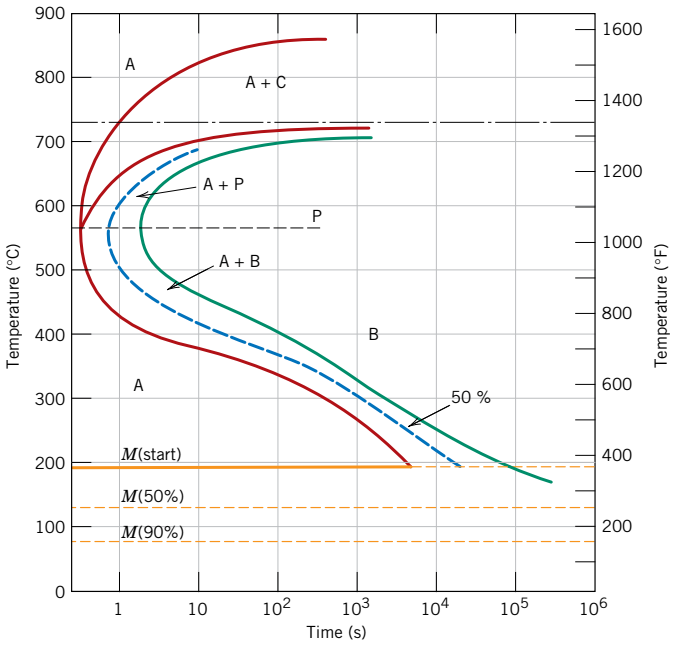

Figure 10.39 Isothermal transformation diagram for a 1.13 wt% C iron–carbon alloy: A, austenite; B, bainite; C, proeutectoid cementite; M, martensite; P, pearlite. [Adapted from H. Boyer (Editor), *Atlas of Isothermal Transformation and Cooling Transformation Diagrams,* 1977. Reproduced by permission of ASM International, Materials Park, OH.]

(g) Rapidly cool to 675°C (1250°F), hold for 7 s, then quench to room temperature.

(h) Rapidly cool to 600°C (1110°F), hold at this temperature for 7 s, rapidly cool to 450°C (840°F), hold at this temperature for 4 s, then quench to room temperature.

10.22 For parts a, c, d, f, and h of Problem 10.21, determine the approximate percentages of the microconstituents that form.

10.23 Make a copy of the isothermal transformation diagram for a 1.13 wt% C iron–carbon alloy (Figure 10.39), and then on this diagram sketch and label time–temperature paths to produce the following microstructures:

(a) 6.2% proeutectoid cementite and 93.8% coarse pearlite

(b) 50% fine pearlite and 50% bainite

(c) 100% martensite

(d) 100% tempered martensite

Continuous-Cooling Transformation Diagrams

10.24 Name the microstructural products of eutectoid iron–carbon alloy (0.76 wt% C) specimens that are first completely transformed to austenite, then cooled to room temperature at the following rates:

(a) 1°C/s

(b) 20°C/s

(c) 50°C/s

(d) 175°C/s

10.25 Figure 10.40 shows the continuous-cooling transformation diagram for a 0.35 wt% C iron–carbon alloy. Make a copy of this figure, and then sketch and label continuous-cooling curves to yield the following microstructures:

(a) Fine pearlite and proeutectoid ferrite

(b) Martensite

(c) Martensite and proeutectoid ferrite

(d) Coarse pearlite and proeutectoid ferrite

(e) Martensite, fine pearlite, and proeutectoid ferrite

10.26 Cite two important differences between continuous-cooling transformation diagrams for plain carbon and alloy steels.

10.27 Briefly explain why there is no bainite transformation region on the continuous-cooling transformation diagram for an iron–carbon alloy of eutectoid composition.

10.28 Name the microstructural products of 4340 alloy steel specimens that are first completely transformed to austenite, then cooled to room temperature at the following rates:

(a) 0.005°C/s

(b) 0.05°C/s

(c) 0.5°C/s

(d) 5°C/s

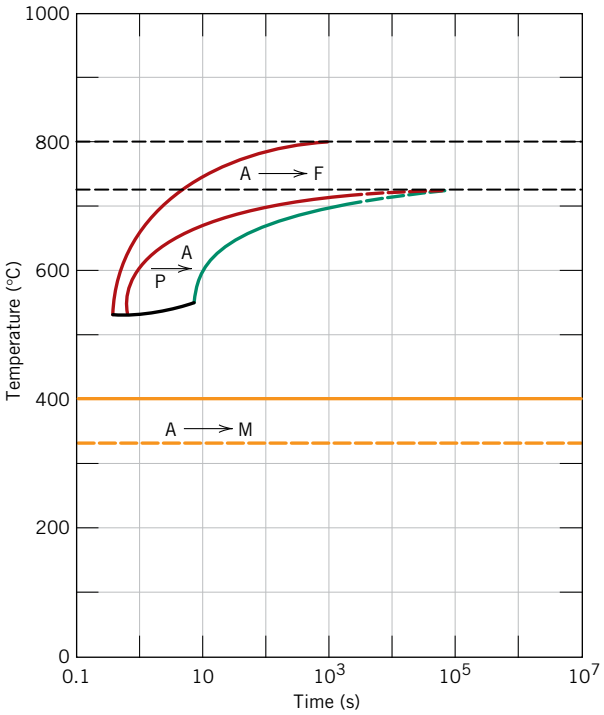

Figure 10.40 Continuous-cooling transformation diagram for a 0.35 wt% C iron–carbon alloy.

10.29 Briefly describe the simplest continuous-cooling heat treatment procedure that would be used in converting a 4340 steel from one microstructure to another.

(a) (Martensite + ferrite + bainite) to (martensite + ferrite + pearlite + bainite)

(b) (Martensite + ferrite + bainite) to spheroidite

(c) (Martensite + bainite + ferrite) to tempered martensite

10.30 On the basis of diffusion considerations, explain why fine pearlite forms for the moderate cooling of austenite through the eutectoid temperature, whereas coarse pearlite is the product for relatively slow cooling rates.

Mechanical Behavior of Iron–Carbon Alloys

Tempered Martensite

10.31 Briefly explain why fine pearlite is harder and stronger than coarse pearlite, which in turn is harder and stronger than spheroidite.

10.32 Cite two reasons why martensite is so hard and brittle.

10.33 Rank the following iron–carbon alloys and associated microstructures from the hardest to the softest:

(a) 0.25 wt% C with coarse pearlite

(b) 0.80 wt% C with spheroidite

(c) 0.25 wt% C with spheroidite

(d) 0.80 wt% C with fine pearlite.

Justify this ranking.

10.34 Briefly explain why the hardness of tempered martensite diminishes with tempering time (at constant temperature) and with increasing temperature (at constant tempering time).

10.35 Briefly describe the simplest heat treatment procedure that would be used in converting a 0.76 wt% C steel from one microstructure to the other, as follows:

(a) Martensite to spheroidite

(b) Spheroidite to martensite

(c) Bainite to pearlite

(d) Pearlite to bainite

(e) Spheroidite to pearlite

(f) Pearlite to spheroidite

(g) Tempered martensite to martensite

(h) Bainite to spheroidite

10.36 **(a)** Briefly describe the microstructural difference between spheroidite and tempered martensite.

(b) Explain why tempered martensite is much harder and stronger.

10.37 Estimate Brinell hardnesses and ductilities (%RA) for specimens of an iron–carbon alloy of eutectoid composition that have been subjected to the heat treatments described in parts (a) through (h) of Problem 10.19.

10.38 Estimate the Brinell hardnesses for specimens of a 1.13 wt% C iron–carbon alloy that have been subjected to the heat treatments described in parts (a), (d), and (h) of Problem 10.21.

10.39 Determine the approximate tensile strengths and ductilities (%RA) for specimens of a eutectoid iron–carbon alloy that have experienced the heat treatments described in parts (a) through (d) of Problem 10.24.

Spreadsheet Problem

10.1SS For some phase transformation, given at least two values of fraction transformation and their corresponding times, generate a spreadsheet that will allow the user to determine the following:

(a) the values of n and k in the Avrami equation

(b) the time required for the transformation to proceed to some degree of fraction transformation

(c) the fraction transformation after some specified time has elapsed

DESIGN PROBLEMS

Continuous-Cooling Transformation Diagrams
Mechanical Behavior of Iron–Carbon Alloys

10.D1 Is it possible to produce an iron–carbon alloy of eutectoid composition that has a minimum hardness of 200 HB and a minimum ductility of 25%RA? If so, describe the continuous-cooling heat treatment to which the alloy would be subjected to achieve these properties. If it is not possible, explain why.

10.D2 For a eutectoid steel, describe isothermal heat treatments that would be required to yield specimens having the following tensile strength-ductility (%RA) combinations:

(a) 900 MPa and 30%RA

(b) 700 MPa and 25%RA

10.D3 For a eutectoid steel, describe isothermal heat treatments that would be required to yield specimens having the following tensile strength-ductility (%RA) combinations:

(a) 1800 MPa and 30%RA

(b) 1700 MPa and 45%RA

(c) 1400 MPa and 50%RA

10.D4 For a eutectoid steel, describe continuous-cooling heat treatments that would be required to yield specimens having the following Brinell hardness-ductility (%RA) combinations:

(a) 680 HB and ~0%RA

(b) 260 HB and 20%RA

(c) 200 HB and 28%RA

(d) 160 HB and 67%RA

10.D5 Is it possible to produce an iron–carbon alloy that has a minimum tensile strength of 620 MPa (90,000 psi) and a minimum ductility of 50% RA? If so, what will be its composition and microstructure (coarse and fine pearlites and spheroidite are alternatives)? If this is not possible, explain why.

10.D6 It is desired to produce an iron–carbon alloy that has a minimum hardness of 200 HB and a minimum ductility of 35% RA. Is such an alloy possible? If so, what will be its composition and microstructure (coarse and fine pearlites and spheroidite are alternatives)? If this is not possible, explain why.

Tempered Martensite

10.D7 **(a)** For a 1080 steel that has been water quenched, estimate the tempering time at 535°C (1000°F) to achieve a hardness of 45 HRC.

(b) What will be the tempering time at 425°C (800°F) necessary to attain the same hardness?

10.D8 An alloy steel (4340) is to be used in an application requiring a minimum tensile strength of 1515 MPa (220,000 psi) and a minimum ductility of 40%RA. Oil quenching followed by tempering is to be used. Briefly describe the tempering heat treatment.

10.D9 For a 4340 steel alloy, describe continuous-cooling/tempering heat treatments that would be required to yield specimens having the following yield/tensile strength-ductility property combinations:

(a) tensile strength of 1100 MPa, ductility of 50%RA

(b) yield strength of 1200 MPa, ductility of 45%RA

(c) tensile strength of 1300 MPa, ductility of 45%RA

10.D10 Is it possible to produce an oil-quenched and tempered 4340 steel that has a minimum yield strength of 1240 MPa (180,000 psi) and a ductility of at least 50%RA? If this is possible, describe the tempering heat treatment. If it is not possible, then explain why.

FUNDAMENTALS OF ENGINEERING QUESTIONS AND PROBLEMS

10.1FE Which of the following describes recrystallization?

(A) Diffusion dependent with a change in phase composition

(B) Diffusionless

(C) Diffusion dependent with no change in phase composition

(D) All of the above

10.2FE Schematic room-temperature microstructures for four iron–carbon alloys are as follows.

Rank these microstructures (by letter) from the hardest to the softest.

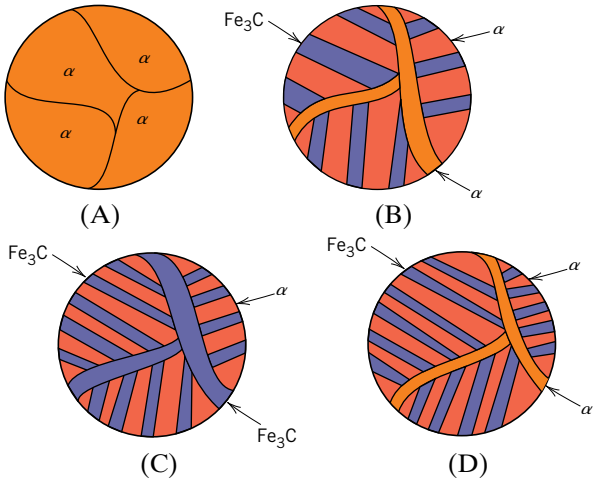

(A) A > B > C > D

(B) C > D > B > A

(C) A > B > D > C

(D) None of the above

10.3FE On the basis of the accompanying isothermal transformation diagram for a 0.45 wt% C iron–carbon alloy, which heat treatment could be used to isothermally convert a microstructure that consists of proeutectoid ferrite and fine pearlite into one that is composed of proeutectoid ferrite and martensite?

(A) Austenitize the specimen at approximately 700°C, rapidly cool to about 675°C, hold at this temperature for 1 to 2 s, and then rapidly quench to room temperature

(B) Rapidly heat the specimen to about 675°C, hold at this temperature for 1 to 2 s, then rapidly quench to room temperature

(C) Austenitize the specimen at approximately 775°C, rapidly cool to about 500°C, hold at this temperature for 1 to 2 s, and then rapidly quench to room temperature

(D) Austenitize the specimen at approximately 775°C, rapidly cool to about 675°C, hold at this temperature for 1 to 2 s, and then rapidly quench to room temperature

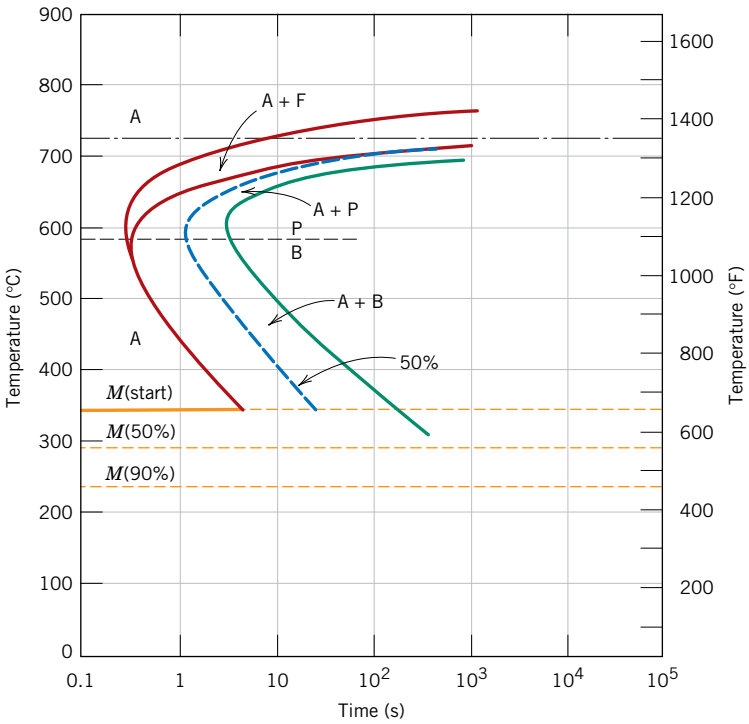

Isothermal transformation diagram for a 0.45 wt% C iron–carbon alloy: A, austenite; B, bainite; F, proeutectoid ferrite; M, martensite; P, pearlite. (Adapted from *Atlas of Time-Temperature Diagrams for Irons and Steels,* G. F. Vander Voort, Editor, 1991. Reprinted by permission of ASM International, Materials Park, OH.)